Kappa Opioid Receptor Antagonism Rescues Genetic Perturbation of Dopamine Homeostasis: Molecular, Physiological and Behavioral Consequences

Felix P Mayer[1,2,%], Adele Stewart[1,2], Durairaj Ragu Varman[3], Amy E Moritz[4], James D Foster[4], Anthony W Owens[5], Lorena B Areal[1], Raajaram Gowrishankar[1#], Michelle Velez[1], Kyria Wickham[1], Hannah Phelps[1], Rania Katamish[1], Maximilian Rabil[1], Lankupalle D Jayanthi[3], Roxanne A Vaughan[4], Lynette C Daws[5,6], Randy D Blakely[1,2]*, Sammanda Ramamoorthy[3]*

[1] Department of Biomedical Science, Charles E. Schmidt College of Medicine, Florida Atlantic University, Jupiter, FL, USA.

[2] Stiles-Nicholson Brain Institute, Florida Atlantic University, Jupiter, FL, USA.

[3] Department of Pharmacology and Toxicology, Virginia Commonwealth University, Richmond, VA, USA

[4] Department of Biomedical Sciences, University of North Dakota School of Medicine and Health Sciences, Grand Forks, ND, USA

[5] Department of Cellular and Integrative Physiology, University of Texas Health Science Center at San Antonio, TX, USA

[6] Department of Pharmacology, University of Texas Health Science Center, San Antonio, TX, USA.

#present address: Departments of Anesthesiology and Pain Medicine and Pharmacology, University of Washington, Seattle, WA, USA and Center for the Neurobiology of Addiction, Pain and Emotion, University of Washington, Seattle, WA, USA

%present address: Department of Neuroscience, Faculty of Health and Medical Sciences, University of Copenhagen, Copenhagen, DK-2200, Denmark.

*to whom correspondence should be addressed:

sammanda.ramamoorthy@vcuhealth.org

rblakely@health.fau.edu

Summary

Aberrant dopamine (DA) signaling is implicated in schizophrenia, bipolar disorder (BPD), autism spectrum disorder (ASD), substance use disorder, and attention-deficit/hyperactivity disorder (ADHD). Treatment of these disorders remains inadequate. We established that the human DA transporter (DAT) coding variant (DAT Val559), identified in individuals with ADHD, ASD, or BPD, exhibits anomalous DA efflux (ADE) that is blocked by therapeutic amphetamines and methylphenidate. As the latter agents have high abuse liability, we exploited DAT Val559 knock-in mice to identify non-addictive agents that can normalize DAT Val559 functional and behavioral effects *ex vivo* and *in vivo*. Kappa opioid receptors (KORs) are expressed by DA neurons and modulate DA release and clearance, suggesting that targeting KORs might offset the effects of DAT Val559. We establish that enhanced DAT Thr53 phosphorylation and increased DAT surface trafficking associated with DAT Val559 expression are mimicked by KOR agonism of wildtype preparations and rescued by KOR antagonism of DAT Val559 *ex vivo* preparations. Importantly, KOR antagonism also corrected *in vivo* DA release and sex-dependent behavioral abnormalities. Given their low abuse liability, our studies with a construct valid model of human DA associated disorders reinforce considerations of KOR antagonism as a pharmacological strategy to treat DA associated brain disorders.

Introduction

Dopamine (DA) is a powerful neuromodulator whose actions impact multiple fundamental behaviors, including novelty and reward salience (1), motivation and attention (2), motor initiation and coordination (3) and executive function (4), among others. Accordingly, altered DA signaling has been implicated in multiple neuropsychiatric disorders including attention-deficit/hyperactivity disorder (ADHD) (5), autism spectrum disorder (ASD) (6), bipolar disorder (BPD) (7), Parkinson's disease (8), schizophrenia (9) and substance use disorders (10), though the detailed molecular underpinnings of these pathological manifestations remain areas of intense investigation. The DA transporter (DAT, *SLC6A3*) mediates the high-affinity uptake of DA and thus tightly regulates the spatiotemporal availability of extracellular DA (11) and aids in replenishing vesicular storages of DA by acting in concert with the *de novo* synthesis machinery (12,13). Abnormal DAT availability in humans with neuropsychiatric disorders has been reported (14,15) and first line treatments for ADHD, i.e., methylphenidate and alpha-methylphenethylamine (amphetamine) formulations (16) exhibit high affinity towards DAT (11) and modulate extracellular DA in human subjects (17). Moreover, given abnormal behavior of DAT-manipulated animals (12,18–24) and that the DAT gene *SLC6A3* is implicated in neuropsychiatric diseases (25), ample evidence identifies DAT as a direct contributor to pathological DA dysregulation.

A role of altered DAT-mediated DA transport in neuropsychiatric disorders has been advanced by the identification of rare missense variants in the *SLC6A3* gene that encodes DAT in individuals diagnosed with ADHD (26–28), BPD (29) and ASD (30–32). Importantly, these variants have been shown to modulate DAT function (27,28,30,33,34) and/or regulated expression of DAT on the cell surface (27,33,35), and thus are expected to perturb extracellular DA clearance *in vivo*. We and colleagues identified the DAT Ala559Val substitution in two male siblings with ADHD (26), and two unrelated males with ASD (32), a disorder with significant ADHD comorbidity (36–38). Grunhage and coworkers also observed expression of the variant in a girl with BPD (29), a disorder also demonstrating significant familial co-morbidity and shared genetics (39,40). When expressed in a heterologous cell model, DAT Val559 displays normal transporter protein expression, surface abundance and DA uptake rates (33,41). Conspicuously, however, the variant exhibits anomalous DA efflux (ADE) when transfected cells are preloaded with DA (41,42) and increased lateral mobility on the cell surface (43), suggestive of alterations in DAT-associated proteins that influence transporter localization and transport dynamics. DAT dependence of DAT Val559-mediated ADE was established through a block of efflux by methylphenidate and amphetamine, as well as cocaine (41,42). Interestingly, ADE has now been recognized as a functional correlate of multiple disease-associated DAT

variants (21,30,34,41,42) and can also be triggered in wildtype (WT) DAT via G protein interactions (44,45), extending the ADE phenotype beyond that seen with rare genetic variants.

To advance the study of DAT Val559 and ADE *in vivo*, we generated and characterized DAT Val559 KI mice (18,46). In striatal preparations from DAT Val559 mice, total DAT expression, DA uptake and tissue DA levels were found to be indistinguishable from those of WT mice (18). In keeping with ADE, however, the striatum of these mice was found to exhibit tonically elevated extracellular DA levels *in vivo* that supports constitutive D2-type autoreceptor (D2AR) activation and blunted vesicular DA release. In keeping with these changes, DAT Val559 mice have been shown to display blunted locomotor responses to methylphenidate and amphetamine, heightened locomotor responses to imminent handling, i.e. darting (18), enhanced motivation for reward and waiting impulsivity (19), altered working memory (24) and compulsive reward seeking (23). Together these findings document the value of DAT Val559 mice as a construct-valid model of endogenous alterations in synaptic DA homeostasis that arise from DAT dysfunction. Moreover, the DAT Val559 model provides an *in vivo* platform for the preclinical evaluation of novel therapeutic strategies to ameliorate synaptic DA-associated neurobehavioral disorders, with a particular need for agents without addictive potential.

On a molecular level, various mechanisms have been identified that modulate DAT activity either via protein-protein interactions (44,47–49) or post-translational modifications (50,51). Of particular relevance to this study, DAT is amenable to regulation via presynaptic receptors, either directly or via G proteins, membrane lipids and protein kinases that mediate receptor signaling effects (42,51–54). For example, DA D_2-type autoreceptors (D2ARs) directly interact with DAT and activation of D2ARs has been shown to promote increased DAT surface trafficking (52,55) via an Extracellular signal-Regulated Kinases 1 and 2 (ERK1/2)-dependent mechanism (52). Notably, as a result of DAT Val559-associated ADE, tonic stimulation of D2ARs recruits efflux prone DAT Val559 to the cell surface (56) resulting in a positive feedback-loop that maintains high levels of DAT-dependent ADE. Interestingly, Gowrishankar and colleagues observed that D2AR-mediated regulation of DAT in male mice is circuit-specific, as this regulation is seen in nigrostriatal DA projections to the dorsal (DS) but not the mesoaccumbal projections to the ventral striatum (VS) (56). Recently, we have found that the circuit specificity of D2AR regulation of DAT is also remarkably sex-specific, with an opposite anatomical pattern of D2AR-DAT coupling seen in female mice, leading to enhanced D2AR-dependent DAT Val559 surface trafficking in the VS, but not in the DS, a difference that likely contributes to the sex-specific changes in behavior observed (24).

Due to the anatomical and sex-specificity of D2AR regulation of DAT, approaches to overcoming ADE through pharmacological D2AR manipulation are likely to present complexities in pharmacological management of DA associated disorders. Targeting DAT to reduce ADE, as with psychostimulants, invokes use of agents with significant abuse liability (57). Thus, we sought an alternative path for DAT modulation that could normalize DAT Val559 phenotypes. In this regard, converging evidence has established a link between kappa opioid receptor (KOR) signaling and the DA system. For example: i) fibers releasing the endogenous KOR agonist dynorphin directly synapse onto DA terminals, where KOR is expressed as a heteroreceptor (58); ii) KOR agonists directly inhibit DA neuron activity (59), which is believed to contribute to stress-related dysphoria (60), resulting from increased secretion of dynorphin during stressful events; iii) acute exposure to agonists of KOR promotes an increase in DAT-mediated DA uptake by promoting surface-trafficking of DAT (54). Lastly, KOR antagonism has been found to be well-tolerated in humans (61–65) suggesting opportunities to modulate DA signaling therapeutically via these agents. For these reasons, we explored KOR signaling manipulation as an approach to mimic or offset the biochemical and behavioral disruptions observed in DAT Val559 mice. In our current report, using transfected cells and native tissue preparations, we found that activation of KOR increases DAT surface trafficking and DAT N-terminal phosphorylation at threonine 53 (Thr53), a site linked to DAT functional regulation and psychostimulant effects (22,66). Conversely, we found that KOR antagonism reduced basal hyperphosphorylation of DAT Thr53 and surface trafficking observed in male DAT Val559 DS and restored normal rates of vesicular DA release. Importantly, KOR antagonism also normalized sex-dependent, DAT Val559-induced perturbations in cognitive and locomotor behavior.

Methods

Materials

Lipofectamine™ 2000, Dulbecco's Modified Eagle Medium (DMEM) and other cell culture media were purchased from Invitrogen/Life Technologies, (Grand Island, NY). [^{3}H]DA (dihydroxyphenylethylamine [2,5,6,7,8-3H], 63.2 Ci/mmol) and Optiphase Supermix, were purchased from PerkinElmer Inc., (Waltham, MA, USA). U69,593, U0126, protease and phosphatase cocktails were obtained from Sigma-Aldrich (St. Louis, MO). Nor-binaltorphimine dihydrochloride (norBNI) was purchased from Tocris (Bristol, United Kingdom). Reagents for SDS-polyacrylamide gel electrophoresis and Bradford protein assays were from Bio-Rad (Hercules, CA, USA), fetal bovine serum and enhanced chemiluminescence (ECL) reagents were from Thermo Fisher Scientific Inc., (Rockford, IL, USA). Sulfosuccinimidyl-2-[biotinamido] ethyi-1,3-dithiopropionate (EZ link NHS-Sulfo-SS-biotin), Protein A magnetic beads (Dynabeads) and NeutrAvidin Agarose were purchased from Thermo Scientific (Waltham, MA, USA). Anti-Calnexin (Cat# ADI-SPA-860-D, RRID: AB-10616095) was obtained from Enzo Life Sciences, Inc (Farmingdale, NY, USA). QuikChange II XL site-directed mutagenesis kit was obtained from Agilent Technologies (Santa Clara, CA, USA). Peroxidase-affinipure goat anti-rabbit IgG antibody (HRP conjugated secondary antibody (Cat# 111-035-003, RRID: AB-2313567) was acquired from Jackson Immuno Research Laboratories (West Grove, PA). DAT antibody Cat# 431-DATC, RRID: AB-2492076 – was used for experiments using EM4 cells. DAT antibody MAB369 (Millipore Sigma, RRID:AB_2190413) -was used for experiments using acute slices). DAT antibody MABN669 (Millipore Sigma, RRID:AB_2717269) was used for experiments in rat striatal synaptosomes. DAT Thr53 Antibody p435-53 (PhosphoSolutions, RRID: AB-2492078) was used to detect DAT phosphorylated at Thr53 in all experiments.

Cell culture and transfection of WT and mutant cDNAs

EM4 cells were maintained in DMEM media with 10% fetal bovine serum, 1% penicillin-streptomycin and 1% glutamine as described previously (54). For DA transport assays, EM4 cells were seeded onto 24 well plates (100,000 cells/well). For surface biotinylation experiments, 150,000 cells/well were seeded onto 12 well plates. After 24 hrs of seeding, cells were co-transfected with cDNA constructs encoding myc-KOR plus rDAT-WT, or myc-KOR plus rDAT Ala53, or myc-KOR plus pcDNA3 using Lipofectamine 2000 according to the manufacturer's instruction. QuikChange II XL site-directed mutagenesis kit was used to alter rat DAT cDNA sequence encoding alanine at amino acid 53 (Ala53) to encode threonine (Thr53). Sequence validation of the substitution and absence of nonspecific mutations were confirmed by sequencing the entire cDNA on both strands.

The following DNA amounts were used for transfections: myc-KOR:0.25 µg/well (24 well plate) 0.5 µg/well (12 well plate); rDAT, or rDAT Ala53: 0.25 µg/well (24 well plate) 0.5 µg/well (12 well plate). Matched amounts of pcDNA3 were transfected for control experiments. The plates were further incubated in a humidified atmosphere at 37˚C and 5% CO_2 for 24 hrs prior to assay.

[^{3}H]DA uptake assay

EM4 cells co-transfected with KOR plus rDAT, or rDAT Ala53, or pcDNA3 in 24 well plates were first washed with serum free DMEM (1 mL/well) media and incubated at 37°C for 2 hrs. Cells were then washed with 1 mL of pre-warmed (37˚C) modified Krebs-Ringer-HEPES (KRH) buffer, pH 7.4 supplemented with L-ascorbic acid and pargyline (10 mM HEPES, 120 mM NaCl, 4.7 mM KCl, 1.2 mM KH_2PO_4, 1.2 mM $MgSO_4$, 10 mM D-glucose, 0.1 mM L-ascorbic acid, 0.1 mM pargyline, pH 7.4). Modulators were added for the times noted in figures and/or legends, followed by the addition of 30 nM [^{3}H]DA to initiate DA uptake. [^{3}H]DA uptake was terminated after 5 min of incubation at 37˚C by removing the uptake mixture and rapidly washing with 1.0 mL KRH buffer three times. Cells were lysed by adding 0.2 mL Optiphase Supermix cocktail and accumulated [^{3}H]DA-radioactivity was measured using a microplate scintillation counter (MicroBeta^2 LumiJET, PerkinElmer, Waltham, MA, USA). DAT- specific [^{3}H]DA transport was calculated as the difference in counts obtained in the presence or absence of the DAT-specific antagonist GBR12909 (100 nM). The effectiveness of GBR12909 in blocking DAT activity was verified using cells transfected with pcDNA3 vector alone. For DAT kinetic analyses, unlabeled DA was mixed with 30 nM [^{3}H]DA, with the final concentration of DA varying from 0.25 µM to 20 µM. Uptake assays were performed in triplicate.

EM4 cell surface biotinylation

Cell surface biotinylation was performed as described previously (54). EM4 cells co-transfected with KOR plus rDAT, or rDAT Ala53, or pcDNA3 in 12 well plates were washed and preincubated with serum free DMEM for 2 hrs followed by treatment with vehicle or U69,593 (10 µM) for 30 min. Biotinylation of cell surface proteins was initiated by incubating cells with EZ link NHS-Sulfo-SS-biotin (1 mg/mL) in cold PBS/Ca^{2+}-Mg^{2+} buffer (138 mM NaCl, 2.7 mM KCl, 1.5 mM KH_2PO_4, 9.6 mM Na_2HPO_4, 1 mM $MgCl_2$, 0.1 mM $CaCl_2$, pH 7.3) for 30 min on ice followed by removal of excess biotinylating reagents by washing the cells twice with ice-cold PBS/Ca^{2+}-Mg^{2+} buffer containing 100 mM glycine and incubated further with glycine (100 mM) for 20 min on ice to quench excess NHS-Sulfo-SS-biotin. The cells were solubilized with 0.7 mL/well of RIPA buffer (10 mM Tris-HCl, pH 7.5, 150 mM NaCl, 1 mM EDTA, 1% Triton X-100, 0.1% SDS, 1% sodium deoxycholate) containing a protease and phosphatase inhibitor cocktail. Surface biotinylated

proteins were isolated from equal amounts of solubilized proteins using NeutrAvidin Agarose resins by overnight incubation at 4˚C followed by washing cells with RIPA. Bound proteins were eluted in 50 µL Laemmli sample buffer (62.5 mM Tris-HCl pH 6.8, 20 % glycerol, 2 % SDS and 5 % ß-mercaptoethanol) by incubating for 30 min at room temp. All eluates and aliquots (40 µl) of total extracts and unbound fractions were used for SDS-PAGE and immunoblot analysis as described below under immunoblot analysis. Proteins were separated using 7.5% SDS-polyacrylamide gels followed by transfer to polyvinylidene difluoride membranes (PVDF, ThermoFisher Scientific). To analyze total DAT and calnexin proteins, membranes were pre-blocked with PBS containing 0.1% Tween 20 and 1% nonfat milk, whereas Tris buffer containing 1% BSA and 0.1% Tween 20 was used for the detection of Thr53-pDAT. Membranes were incubated with primary antibodies to DAT or Thr53-pDAT (1: 1000) overnight at 4˚C. After washing, secondary antibody peroxidase-affinipure goat anti-rabbit IgG antibody (1: 10,000) was incubated for 1 hr at room temp followed by detection of immunoreactive proteins using ECL or ECL plus reagent (ThermoFisher Scientific). Using NIH Image J 1.52a, bands were quantified from digitized blots within the linear range of the film exposure. Specific nature of DAT bands was defined by the absence of corresponding immunoreactive signal in pcDNA3 transfected cells analyzed in parallel. Blots were also stripped and reprobed with calnexin antibody(1:10000 dilutions) to normalize total DAT and p-Thr53 DAT.

Animals

All procedures involving animals were approved by the Institutional Animal Care and Use Committees of UT San Antonio Health Sciences Center, Virginia Commonwealth University, or Florida Atlantic University depending on the site of assays, in accordance with the National Institutes of Health Guide for the Care and Use of Laboratory Animals. Male Sprague-Dawley rats (175-350 g body weight) were utilized for *in vivo* chronoamperometry and assays of DAT Thr53 phosphorylation in synaptosomes and tissue. For slice experiments, age-matched 4- to 6-week-old male homozygous mice for either WT or DAT Val559 (genetic background: 75% 129/6 and 25% C57; (18)) were bred from homozygous dams and sires that were derived from heterozygous breeders. Male mice were used due to the male bias observed in ADHD diagnosis (67). All biochemical experiments were conducted during the light phase. For behavioral experiments, 6–8-week-old WT and homozygous DAT Val559 littermates derived from heterozygous breeders were utilized. Male mice were used for all behavioral experiments except the novel object recognition test due to the demonstrated sex bias of behavioral phenotypes observed in DAT Val559 mice (24). Behavioral testing was performed during the dark phase of the light cycle under red light. Rodents were maintained in a temperature and humidity-controlled room on a 12:12 h light/dark cycle. Food and water were supplied

ad libitum. All efforts and care were taken to minimize animal suffering and to reduce the number of animals used. As alternatives to brain tissues, cell culture models were utilized.

Treatment of striatal synaptosomes with U69,593 ± U0126

Male Sprague-Dawley rats (175–300 g) were decapitated, and striata were rapidly dissected, weighed, and placed in ice-cold sucrose phosphate (SP) buffer (0.32 M sucrose and 10 mm sodium phosphate, pH 7.4). Tissues were homogenized in ice-cold SP buffer with 15 strokes in a glass/Teflon homogenizer and centrifuged at 3000 × *g* for 3 min at 4 °C. Supernatant fractions were re-centrifuged at 17,000 × *g* for 12 min, and the resulting P2 pellet enriched for synaptosomes was resuspended to 20 mg/mL original wet weight in ice-cold SP buffer. Synaptosomes were treated with vehicle or 50 µM U0126 for 15 min at 30˚C, followed by treatment with vehicle or 10 µM U69,593 for an additional 15 min at 30˚C. After treatment, samples were subjected to SDS-PAGE followed by immunoblotting for total DAT and DAT phosphorylated at Thr53 (p-Thr53 DAT levels).

p-Thr53 DAT levels from rats injected with vehicle or U69,593

Male rats were injected s.c. with vehicle or 0.32 mg/kg U69,593 and sacrificed at the indicated times noted in Figure 3. DS or VS were dissected, weighed and kept frozen until analyzed. The pre-weighed samples were homogenized with a Polytron PT1200 homogenizer (Kinematica, Basel, Switzerland) for 8 s in ice-cold SP buffer, and centrifuged at 3000 *× g* for 3 min at 4 °C. Supernatant fractions were re-centrifuged at 17,000 *× g* for 12 min to obtain a membrane pellet. The pellet was resuspended to 20 mg/mL original wet weight in ice-cold SP buffer. Samples were subjected in duplicate to SDS-PAGE and western blot for total and p-Thr53 DAT, and p-Thr53 DAT staining quantified by normalization to the time-matched controls.

Analysis of in vivo DA clearance in NAc

High-Speed *in vivo* chronoamperometry, conducted as previously described (68), was used to determine the effect of KOR modulators on DA clearance in NAc of anesthetized rats. Briefly, carbon fiber electrodes were attached to multi-barrel glass micropipettes. The tips of carbon fibers (150 µm in length) were coated with 5% Nafion to provide a 1000-fold selectivity of DA over its metabolite dihydroxyphenylacetic acid (DOPAC) and displayed linear amperometric responses to 0.5 – 10 µM DA during *in vitro* calibrations. Rats were anesthetized with chloralose (85 mg/kg, i.p.) and urethane (850 mg/kg, i.p). Electrodes were lowered into the NAc (Anterior/Posterior, +1.7 mm relative to bregma; medial/lateral, ±0.9 mm relative to bregma; V, -6.0 mm from dura; (69)using a stereotaxic frame. Throughout the experiments, body

temperature was maintained at 37 ±1°C by a water-circulated heating pad. Individual micropipette barrels were filled with DA (200 µM), U69,593 (885.7 µM, barrel concentration), norBNI (400 µM, barrel concentration) and vehicle and ejected (100–150 nL) using a Picospritzer II (General Valve Corporation, Fairfield, NJ), to deliver 89 to 134 pmol U69,593, or 40 to 60 pmol norBNI. Note that there is a 10-200 fold dilution in the concentration of drug reaching the area surrounding the recording electrode (68), thus concentrations of U69,593 and norBNI at the recording electrode are estimated to range from 5 to 89 µM, and 2 to 40 µM, respectively. Oxidation potentials consisted of 100 ms pulses of +0.55 V alternated with 100 ms intervals during which the resting potential was maintained at 0 V. Oxidation and reduction currents were digitally integrated during the last 80 ms of each 100 ms voltage pulse. DA was pressure-ejected until a stable baseline signal was established (typically after 3-4 ejections). The effect of U69,593, norBNI, and vehicle on DA signals was quantified 2 min after a stable baseline DA signal was established. Changes in T50 (time required for the signal to decline by 50% of its peak amplitude) and T80 (time required for the signal to decline by 80% of its peak amplitude) were used to determine the influence of U69,595 (KOR activation) and norBNI (KOR inhibition) or vehicle on DA clearance.

Surface biotinylation and immunoprecipitation of p-Thr53 DAT using acute mouse brain slices

All procedures were performed as described previously (Gowrishankar et al., 2018).

Acute slice preparation: Male 4-6 week-old mice were sacrificed by rapid decapitation, brains were removed and transferred into ice-cold oxygenated sucrose artificial cerebrospinal fluid (sucrose-aCSF; in mM: sucrose 250, KCl 2.5, NaH_2PO_4 1.2, $NaHCO_3$ 26, D-glucose 11, $MgCl2.6H_2O$ 1.2, $CaCl_2.2H_2O$ 2.4, pH 7.4, 300 –310 mOsm), Subsequently, 300 µm thick coronal slices (Anterior/Posterior: 1.5-1.0 mm for the ventral striatum; 1.0-0.2 mm for the dorsal striatum) were collected using a Leica VT100 S vibratome in ice-cold oxygenated sucrose-aCSF. Slices were then allowed to recover at 30-32 °C for 45-60 min in standard aCSF (in mM: NaCl 124, KCl 2.5, NaH_2PO_4 1.2, $NaHCO_3$ 26, D-glucose 11, $MgCl_2.6H_2O$ 1.2, $CaCl_2.2H_2O$ 2.4, pH 7.4, 300 –310 mOsm) with constant oxygenation. Afterwards, slices were transferred to a water bath kept at 37 °C and washed three times with standard aCSF (5 min each) before drugs or vehicle were added (U69,593: 10 µM for 7 min. norBNI: 1 µM for 20 min) with constant oxygenation. After drug treatments, the slices were subjected to three rapid washes and two 5-min washes with ice cold oxygenated standard aCSF. For immunoprecipitation studies, VS and DS were dissected at this point and tissue was flash frozen in liquid nitrogen and stored at -80 °C until processed. For biotinylation experiments, the slices were exposed to 1 mg/mL EZ link NHS-Sulfo-SS-biotin for 30 min on ice with constant oxygenation. Subsequently, the reaction was quenched by exposing the slices to 0.1 M glycine

(in standard-aCSF; two 10 min incubations). Finally, slices were washed with ice-cold standard-aCSF (three rapid and two 5-min washes) and ventral and dorsal striatum were dissected and transferred into RIPA buffer (in mM: Tris-HCl 25 pH 7.6, NaCl 150, EDTA 5, 1% Triton X-100, 1% sodium deoxycholate, 0.1% SDS) supplemented with protease inhibitor cocktail (P8340, Millipore Sigma; used at a 1:100 dilution). Tissue was solubilized by passing the slices through a 29 gauge needle and nutation at 4 °C for 60 min. Subsequently, samples were centrifuged at 4 °C for 15 min at 21,000 *x g*, pellets were discarded, and supernatants transferred into fresh tubes. Subsequently, protein concentrations were determined using the BCA protein assay (ThermoFisher) and assessed with a FLUOstar Omega microplate reader (BMG Labtech). Bovine serum albumin was used as standard. Lysates were exposed to Pierce™ Streptavidin Agarose beads (ThermoFisher; 20353) (ratio: 20 µg of protein to 50 µL bead slurry) (minimum 2 hrs, maximum 12 hrs) under constant nutation. Beads were washed 3 times with RIPA buffer and protein was eluted and denatured by adding 2X sample buffer (0.5 mM Tris-HCl pH 6.8, 25% glycerol, 1.0% bromophenol blue, 10% SDS, 5 % beta-mercaptoethanol) at room temp for 30 min on a shaker. 5 µg of total protein was loaded on the same gel to normalize the surface DAT to total DAT present in each sample.

Immunoprecipitation: Slices were transferred into ice-cold lysis buffer (in mM: NaCl 138, KCl 2.7, TRIS 50, 1% Triton X-100, pH 8) supplemented with protease (P8340, Millipore Sigma) and phosphatase (P0044, Millipore Sigma) inhibitors (both used at a 1:100 dilution). Tissue was solubilized by carefully passing the slices through a 29 Gauge needle and subsequent nutation at 4 °C for 60 min. Samples were centrifuged at 4 °C for 15 min at 21000 *x g*, pellets were discarded and supernatants transferred into fresh tubes. Rabbit Thr53 DAT antibody (RRID:AB_2492078) was crosslinked to protein A magnetic beads (Dynabeads, ThermoFisher; ratio 1 µL Thr53 antibody:10 µL Dynabeads as described (56). 20 µL of DAT Thr53 antibody-conjugated beads were added to 200 µg of protein and nutated (minimum 4 hrs, maximum 10 hrs) at 4 °C. Subsequently, beads were washed with lysis buffer (4 times) and incubated with 50 uL of 2X sample buffer (0.5 mM Tris-HCl pH 6.8, 25% glycerol, 1.0% bromophenol blue, 10% SDS, 5 % beta-mercaptoethanol) for 45-60 min at room temp on a shaker to elute/denature protein before SDS-PAGE and immunoblotting for DAT. 5 µg of total protein was loaded on the same gel to normalize the immunopurified p-Thr53 DAT to total DAT present in each sample.

Behavioral testing

Y Maze and Open Field Testing – On day 1, 6–8-week-old WT and homozygous DAT Val559 male mice received a single injection of saline or norBNI (10 mg/kg, i.p.) 30 mins prior to behavioral testing and were returned to their home cage until experiment initiation. Animals were subsequently placed in a Y-shaped maze combining 3 white, opaque plastic arms (14 × 4.5 × 40 cm) each at a 120°C angle from the others. Each subject was introduced to the center of the maze and allowed to freely explore all arms for 10 min. Locomotor activity and arm entries were monitored using Ethovision XT video tracking software (version 15; Noldus, Leesburg, VA) and the percent alternation calculated as the number of alternations (incidences where animals visited each arm in turn without repeating an arm) divided by the total number of arm visit triads X 100. 1 week later, animals were again placed in the maze to assess whether drug and genotype effects were maintained in accordance with the long lasting effects of norBNI (70,71). 2 days after the second Y Maze test, the same animals were placed in an open field apparatus (27 cm X 27 cm x 20.5 cm) contained within light- and air-controlled sound-attenuating boxes (Med Associates, Fairfax, VT). As described previously (24), locomotion (horizontal/vertical) as well as stereotypic behaviors and center occupancy were detected by interruption of a grid of infrared beams (16 photocells in each horizontal axis and elevated 4 cm above the floor). Data were collected and analyzed by Med Associates Activity Monitor software.

Cocaine-induced locomotor activation - To assess the effect of norBNI on cocaine-induced locomotor activity, 6–8-week-old WT and homozygous DAT Val559 DAT male mice were injected with norBNI (10 mg/kg, i.p.) one week prior to the open field test and then received either saline or cocaine (Sigma, 10 mg/kg, i.p.) immediately prior to placement in Med Associates open field apparatuses. Locomotor activity was collected for 60 minutes following drug injection utilizing Med Associates Activity Monitor software as above.

Novel Object Recognition (NOR) test - The novel object recognition (NOR) test was performed as described in Stewart et al., 2022 (24). Female WT and DAT Val559 mice (6-8 weeks of age) were utilized for this test as the behavior of DAT Val559 males is unaltered relative to WT littermates (24). Mice were habituated to the test apparatus for 10 min once per day for 2 days. On day 3, mice received a single injection of saline or norBNI (10 mg/kg, i.p.) 30 mins prior to placement in the test apparatus with two identical objects. Given that norBNI impacts are long lasting, mice were not re-dosed on day 4 when they were allowed to freely explore a familiar object or novel object. Activity was monitored with Ethovision XT

software (version 15) and data are presented as % time exploring each object or discrimination index [(time with novel object – time with familiar object)/total exploration time].

In vivo microdialysis

Surgeries to insert microdialysis guide cannulae were performed as described earlier (18,72). 6–8-week-old male mice were anesthetized using isoflurane (5 % induction/ 2 % maintenance) and their heads were fixed in a stereotaxic frame. Ophthalmic ointment was applied to prevent drying of the eyes. Analgesics: bupivacaine and lidocaine were administered locally (100 µL of sterile saline containing 0.05% bupivacaine and 0.2% lidocaine, subcutaneous injection (s.c.)) and ketoprofen (10 mg/kg, s.c.) was administered systemically. Following a midline incision, lambda and bregma were levelled and a craniotomy was performed using a dental drill. Microdialysis was performed as described in Mergy et al., 2014 (18), with minor modifications: a 5 mm guide cannula (S-5000; Synaptechnology Inc., Marquette, MI) was lowered into the DS using the following target coordinates (referring to the tip of the guide cannula): Anterior/Posterior 0.86 mm, Medial/Lateral 1.6 mm, Dorsal/Ventral - 2.3 mm (all relative to bregma). The guide cannula was affixed to the skull with dental cement, supported by three 1.6 mm screws (Plastics One Inc., 00-96X1/16 39052; Fisher Scientific). Subsequently, mice were allowed to recover for 6 days. 12 hr prior to the experiment a microdialysis probe with an active membrane length of 3 mm (S-5030; Synaptechnology Inc., Marquette, MI) was inserted into the guide cannula and mice were placed into 15 inch high, plexiglass recording chambers (MTANK W/F (Instech, Plymouth Meeting, PA, USA)) with bedding and food and water provided *ad libitum*. The probe was superfused with artificial cerebrospinal fluid (in mM: NaCl 149, 2, KCl 2.8, $CaCl_2$ 1.2, $MgCl_2$ 1.2, and D-glucose 5.4, pH 7.2) overnight (12h) at a flow rate of 1 µL per min before the collection of dialysates was initiated. 20 min fractions were collected on ice and stored at -80 °C until they were analyzed with HPLC-EC (Neurobehavior Core, FAU Stiles-Nicholson Brain Institute). After collection of the three (0-60 min) baseline fractions, mice received an i.p. injection of norBNI (10 mg/kg). After four additional fractions, cocaine hydrochloride (10 mg/kg; i.p.) was injected. Changes in extracellular DA were expressed as fold increase of basal DA (i.e. the average DA of the first three basal dialysates).

Statistical analyses

Prism 7 (GraphPad, San Diego, CA) was used for data analysis and graph preparation. Values are presented as mean ± standard deviation (SD). One-way or two-way ANOVA were used followed by post hoc testing for multiple comparisons. The type and results of post hoc tests are noted in the Figure legends. Two-

tailed, unpaired Student's t-tests were performed for comparisons between two groups. P values ≤ 0.05 were considered statistically significant.

Results

KOR-agonist treatment affects rDAT mediated DA uptake in transfected EM4 cells in a concentration and time-dependent manner

To initiate our evaluation of KOR manipulation as a strategy for offsetting DAT-dependent alterations in DA homeostasis, we transiently transfected EM4 cells with rat cDNAs encoding KOR and DAT (rKOR and rDAT), respectively. We found that treatment with the KOR agonist U69,593 augmented DA-uptake into these cells in a concentration (Figure 1A) and time-dependent (Figure 1B) manner, effects that were eliminated with the KOR antagonist norBNI (Suppl. Figure 1). These findings are in agreement with a previous study, showing that activation of KOR enhances DAT-mediated uptake (54). We selected 10 µM U69,593 and a 15 min pre-treatment for subsequent *in vitro* experiments. Through DA uptake saturation experiments, and in agreement with the findings of Kivell et al (2014), a 15 min pre-treatment with 10µM U69,593 significantly increased DA transport V_{max} (336.1 ± 18.12 versus 551.2 ± 21.79 pmol/min/10^6 cells), whereas DA K_M was unaffected (Figure 1C).

KOR regulation of DAT activity requires the capacity to phosphorylate DAT at Thr53 in the DAT N-terminus

The site(s) or motifs in DAT through which KOR regulates DAT function have not been defined. Comprehensive research has identified DAT phosphorylation as a key mechanism that determines DAT activity and membrane trafficking (51,73,74), with work to date focusing on phosphorylation of N- and C-terminal cytoplasmic domains. We focused on the N-terminus due to evidence that the MAP kinase ERK1/2 supports KOR regulation of DAT (54) and a conserved, N-terminal proline-directed kinase consensus phosphorylation motif containing Thr53 that can be phosphorylated in *vitro* by ERK1 (75) has been implicated in DAT function (66,76). Moreover, mice lacking the capacity to phosphorylate Thr53 are insensitive to ERK1/2 inhibitors (77). To initiate this effort, we first generated two truncated versions of rDAT, lacking either the first 22 (Δ1-22) or 55 (Δ1-55) N-terminal residues. Despite the loss of multiple phosphorylation sites that are found within the most distal N-terminus (51,74), we found that rDAT Δ1-22 remained amenable to regulation via activation of rKOR, as treatment with U69,593 significantly increased DA uptake in EM4 cells coexpressing rDAT ΔN1-22 and rKOR (Figure 1D). In contrast, no uptake stimulation by U69,593 was evident in cells transfected with rKOR and rDAT ΔN1-55. Given the evidence discussed above as to a likely role of Thr53 phosphorylation (p-Thr53) to rDAT function, and the fact that Thr53 is located in the region that distinguishes ΔN1-55 from Δ1-22, we replaced Thr53 with an alanine (rDAT Ala53) to preclude phosphorylation at this site. Single point and saturation uptake analyses in EM4 cells transfected with rKOR and either WT rDAT or rDAT Ala53 revealed an absolute requirement for Thr53

phosphorylation potential for U69,593 to increase DA uptake (Figure 1E-F). Saturation analysis also demonstrated that a reduction in V_{max} supports the basal reduction in rDAT Ala53 DA uptake (124.4 ± 18.45 (SD) pmol/min/10^6cells)) evident in comparison to WT rDAT (337.4 ± 57.65 (SD) pmol/min/10^6cells) (Figures 1C, 1F).

KOR agonism increases rDAT surface levels in a Thr53-dependent manner in EM4 cells

Given the well-established relationship between DAT surface expression and DA uptake, we next sought to determine whether the Thr53-dependent KOR elevation of rDAT-mediated uptake correlates with an increase in transporter surface expression. To pursue this objective, we biotinylated transfected cells with the membrane-impermeant reagent EZ link NHS-Sulfo-SS-biotin and recovered surface-enriched DAT proteins from total protein extracts as noted in Methods. Exposure of cells to U69,593 as in uptake studies had no effect on total levels of either WT rDAT or rDAT Ala53 (Figure 2A). Western blots of total extracts revealed WT rDAT to migrate as distinct bands of ~55-60 kDa and ~85-90 kDa, typical of rDAT transiently transfected cells and linked to different transporter species bearing mature versus immature states of N-glycosylation (78). In contrast to the WT rDAT protein profile, extracts from cells expressing the DAT Ala53 mutant were depleted of the 85-90 kDA species. No bands were detected in pcDNA3-transfected cells (Figure 2A), indicative of the specificity of the DAT antibody used in our studies. Analysis of rDAT species in biotinylated samples showed that U69,593 significantly increased WT rDAT surface density for both the ~55-60 kDa and ~85-90 kDa DAT bands. In contrast, neither species of rDAT Ala53 was affected by U69,593 treatment (Figure 2B). To detect rDAT Thr53 phosphorylation (p-Thr53), we probed blots with a DAT p-Thr53 specific antibody (66). We found that U69,593 treatment significantly increased immunoreactivity for the ~85-90 kDa isoform of DAT p-Thr53 labelled proteins in total extracts from WT rDAT transfected cells, whereas increased DAT p-Thr53 labelling of the WT rDAT ~55-60 kDa isoform was not detected. Importantly, no DAT-specific bands of either isoform were detected in surface-samples from cells transfected with the rDAT Ala53 variant (Figure 2C). Finally, when we analysed blots from extracts recovered after surface biotinylation, we detected a significant increase in DAT p-Thr53 immunoreactivity for both isoforms of WT DAT, whereas no DAT p-Thr53-specific bands were detected in the case of the Ala53 variant (Figure 2D). Of note, the DAT p-Thr53 antibody detected some non-specific bands, which were also present in mock-transfected cells (* in Figures 2C and D) and therefore not considered for analysis. Together, our findings indicate that capacity for Thr53 phosphorylation is essential for enhanced surface trafficking of rDAT in response to rKOR agonism in EM4 cells.

Pharmacological activation of KOR increases rDAT phosphorylation at Thr53 in striatal synaptosomes and enhances DA clearance in vivo

Having established in transfected cells that a capacity for rDAT Thr53 phosphorylation plays an essential role of in KOR-dependent elevations of transporter surface trafficking and DA uptake, we next sought to determine whether these findings could be replicated in native tissue. As shown in Figure 3A, treatment of rat striatal synaptosomes with U69,593 promoted a significant increase in p-Thr53 DAT immunoreactivity that could be blocked by inhibition of mitogen-activated protein kinase kinase (MEK1/2) using U0216, which lies upstream of ERK 1/2 (Figure 3A). To assess whether KOR activation can elevate p-Thr53 DAT *in vivo*, male rats were injected with U69,593 (0.32 mg/kg, i.p.) or vehicle and sacrificed at the time points shown in Figure 3B and C. To parse out whether circuit-specific effects that shape the outcome of D2AR regulation of DAT surface trafficking (24,56) also exist for KOR, we analysed the impact of systemic U69,593 on p-Thr53 DAT by western blot in both the DS (Figure 3B) and VS (Figure 3C). For both DS and VS, systemic U69,593 caused a time-dependent increase in p-Thr53 DAT that peaked at 120min post injection. Considering the effects of KOR activation to increase DAT-mediated DA uptake in cells (Figure 1 and previously published reports;(54)), we sought *in vivo* evidence for increased DAT function following KOR activation via assessment of DA clearance time using high-speed *in vivo* chronoamperometry (68,79). As described in Methods, a carbon fiber electrode-micropipette assembly was lowered into the NAc (Figure 3D) permitting DA to be pressure ejected, followed by recording of DA levels as a function of time. Representative traces depicting DA clearance before and after administration of U69,593 are shown in Figure 3E. We found that local injection of U69,593 decreased DA clearance time compared to predrug baseline, quantified as the time required to clear 50% (T50) and 80 % (T80) of the DA-induced amperometric signal (Figure 3F). In contrast, pre-treatment with the KOR antagonist norBNI significantly increased clearance time consistent with a non-saturating level of endogenous KOR activation under our recording conditions (Suppl. Figure 2).

Targeting KOR to normalize aberrant surface trafficking and phosphorylation of the disease associated DAT variant DAT Val559 in vivo

We have previously shown that DAT Val559, owing to its generation of ADE, gives rise to biochemical, physiological and behavioral alterations *in vivo* as monitored in DAT Val559 mice. Importantly, DAT Val559 expression in male mice is associated with increased surface trafficking of DAT and elevated levels of p-Thr53 DAT in the DS but not the VS due to tonic activation of presynaptic D2Ars (56). The ability noted above of endogenous rKORs to regulate rDAT-dependent DA clearance raised the possibility that

pharmacological antagonism of mKORs in DAT Val559 mice might be able to normalize the tonically elevated surface expression of efflux-prone mDAT Val559 proteins, and thereby normalize the behavioral disturbances observed in the model. To determine whether mDAT Val559 remains amenable to regulation via mKOR in native brain preparations, we first treated acute coronal slices containing either DS or VS of WT mDAT or mDAT Val559 *in vitro* with U69,593 (10 µM, 7 min) as described in Methods, extracting DAT proteins thereafter for analysis of transporter surface trafficking and p-Thr53 levels via western blots. With respect to surface density (Figure 4B, E), we found that, as previously described (56), extracts from slices generated from the mDAT Val559 DS (Figure 4B), but not the VS (Figure 4E), demonstrated significantly enhanced surface transporter levels under basal conditions, as compared to levels found with extracts of WT mDAT slices. *In vitro* activation of mKOR increased surface trafficking of transporters independent of genotype in both the DS (Figure 4B) and VS (Figure 4E). As with surface transporter density, and as previously reported (Gowrishankar et al, 2018), blots of mDAT Val559 extracts from male DS (Figure 4C) but not VS (Figure 4F), demonstrated significantly elevated levels of p-Thr53 DAT under vehicle-treated conditions. Whereas U69,593 (10 µM, 7 min) increased levels of p-Thr53 DAT in extracts both from DS (Figure 4C) and VS (Figure 4F) of WT male mice as well as VS from DAT Val559 male mice (Figure 4 E), this effect was blunted in male DAT Val559 preparations from the DS (Figure 4C), suggesting a possible ceiling effect for DAT Thr53 phosphorylation. Together, these data suggest that mDAT and mDAT Val559 are both amenable to regulation via KOR in native tissue preparations.

Based on the ability of the KOR antagonist norBNI to diminish DA clearance in WT rats *in vivo*, we reasoned that if tonic stimulation of KORs occurs in mouse brain slices, *in vitro* application of norBNI could oppose the effects of tonic D2AR activation in the DAT Val559 DS produced by ADE. Whereas we found that norBNI (1 µM, 20 min) produced no effect on either surface density or DAT p-Thr53 levels when applied to WT DAT DS slices, norBNI normalized the elevations observed in both transporter surface density (Figure 5B) and p-Thr53 DAT (Figure 5C) in the DS of DAT Val559 mice. In the VS, norBNI was without effect on transporter trafficking or p-Thr53 levels of either WT or DAT Val559 mice (Figure 5 E and F).

In vivo KOR antagonism rescues vesicular DA release and behavioral deficits in DAT Val559 mice

Having observed the ability of norBNI to rescue mDAT Val559-induced elevations in both mDAT Thr53 phosphorylation and surface expression in acute brain slices, we sought to determine whether KOR antagonism *in vivo* could normalize behavioral changes observed in the mutant mice. Our previous *ex vivo* studies with striatal slices revealed a significant reduction of evoked vesicular release of DA from male

DAT Val559 mice (18). Subsequent studies using *in vivo* microdialysis in the DS of these animals revealed a loss of cocaine (10 mg/kg, i.p.) induced DA release (20) consistent with tonic D2AR activation and D2AR-mediated suppression of vesicular DA release. We hypothesized that mKOR inhibition, due to its ability to reduce the elevated basal surface trafficking of efflux-prone mDAT Val559 should diminish basal extracellular DA levels and thereby reduce tonic D2AR-dependent inhibition of vesicular DA release. Indeed, as shown in Figure 6A-B, when male mice were treated with norBNI (10 mg/kg; i.p.) 30 min prior to an i.p. injection of cocaine (10 mg/kg), we found that cocaine now evoked a robust increase in extracellular DA in DAT Val559 mice, equivalent to that seen with WT mice (Figure 6 A-B).

To determine whether a restoration of vesicular DA release might lead to a normalization of behaviors found to be disrupted in DAT Val559 mice, we chose the Y-maze test of spontaneous alternation, a measure whose reduction is considered a symptom of disrupted working memory or compulsive repetitive behavior. Previously, we found that male but not female DAT Val559 mice display a robust reduction in alternations in the Y maze, when compared to WT littermates, driven by immediate return to a previously visited arm (direct revisits) (24). In our current study, we confirmed these observations (Figure 7A through F and (24), finding them also to be driven by increased revisits to the last visited arm (Suppl Fig 3A and B) that was not explained by changes in locomotor activity (Figure 7C,F). Strikingly, an acute injection of norBNI (10 mg/kg, i.p. 30 min prior to initial Y maze testing) normalized the alternation deficit of DAT Val559 mice (Figure 7B) as well as the direct revisits monitored in the task (Suppl Figure 3A) without an effect on locomotor behavior (Figure 7 C). NorBNI is associated with long lasting effects *in vivo* (70,71). Therefore, we reassessed Y maze activity in the same experimental subjects as reported above, one week after the initial test. As expected, one week following the initial study, the vehicle treated DAT Val559 mice continued to display an increase in direct revisits when compared to WT controls (Supplementary Figure 3B). The norBNI treated DAT Val559 group exhibited a direct revisit pattern that was statistically indistinguishable from vehicle treated WT controls (Suppl Fig 3B). Moreover, the norBNI treated DAT Val559 mice displayed a significantly altered alternation pattern when compared to vehicle treated DAT Val559 mice (Figure 7 E). Similarly, we also found no drug or genotype effect on total distance travelled during the Y maze test sessions one week post norBNI treatment (Figure 7F).

Unlike DAT KO mice (12), male (or female) DAT Val559 mice are not spontaneously hyperactive, though male DAT Val559 mice have been found to display increased locomotor reactivity (darting) in response to imminent handling (18). During open field testing, we noted that male DAT Val559 mice displayed

locomotor suppression (distance travelled, rearing and stereotypy) in the open field chamber, as compared to WT littermates, suggestive of heightened anxiety following repeated handling (Figure 8A,B). Remarkably, a single injection of norBNI 7 days prior prior to testing normalized these measures (Figure 8D,E). We hypothesize that the reduced locomotion of the saline treated DAT Val559 mice may represent heightened anxiety post handling. Indeed, DAT Val559 mice demonstrated reduced center time in the open field (Fig 8C), a behavioral measure known to be responsive to anxiolytics (Prut, 2003- 12600700). Systemic norBNI also normalized this measure (Figure 8C). Additionally, DAT Val559 mice display a blunted locomotor response to psychostimulants, including cocaine (10 mg/kg, i.p.) (18,20). Pretreatment with norBNI (10 mg/kg, i.p.) one week prior to testing restored the locomotor response of male DAT Val599 mice to systemic cocaine. In the norBNI treated group, the increase in cocaine-induced locomotor activity was concomitant with an increase in time spent in the center of the chamber, with the latter measure being absent in saline treated controls (Figure 8 F and G).

Our recent efforts have revealed that DAT Val559 affects dopaminergic circuits in a sex-dependent manner that leads to distinct behavioral outcomes in males versus females (24). To determine if systemic treatment with norBNI (10 mg/kg, i.p.) is also capable of reversing a female-specific phenotype of DAT Val559 expression, we implemented the novel object recognition (NOR) test, where female but not male DAT Val559 mice display strong differences in novel object preference and discrimination, as we have previously observed that female DAT Val559 mice do not explore a novel object to the same extent as WT controls (Stewart 2022). Again, treatment with norBNI (10 mg/kg, i.p.) restored the discrimination index and time spent with the novel object of female DAT Val559 mice to levels that were comparable to those observed in female WT mice (Figure 9A through C). Importantly, deficits in the relative interaction time (Figure 9B) and discrimination index (Figure 9C) are not confounded by locomotor activity (Figure 9D) or total object interaction time on testing day 1 (Figure 9 E) or testing day 2 (Figure 9F), as all these measures remained unchanged in female DAT Val559 mice. Consequently, these findings demonstrate that mKOR antagonism can normalize behavioral changes unique to either male or female DAT Val559 mice.

Discussion

Dysfunction in DAergic signaling has been linked to multiple neuropsychiatric disorders including ADHD (80), schizophrenia (81) and ASD (82). Detailed understanding of DA-linked processes is required for the development of effective strategies to treat disorders that feature deficits in DA neurotransmission. At a synaptic level, the extracellular availability of DA is shaped by two opposing processes: release and inactivation of DA. The impact of intact clearance of released DA on its extracellular levels is evidenced by the fact that DA remains 100-times longer in the extracellular space when DAT expression is genetically precluded (12). Initial efforts to model disturbed DA-signaling primarily aimed to disrupt vesicular release (83), reuptake (12) or synthesis of DA (84) using knock-out animals. The KO model suffers, however, from issues related to construct validity with respect to most DA-linked neurobehavioral disorders as homozygous loss-of-function DAT mutations in humans exhibit Juvenile Dystonia/Parkinsonism and require intensive support to live past early childhood (85,86). The discovery of rare DAT-coding variants in subjects diagnosed with ADHD (26–28,31), ASD (30,32), , BPD (29) both substantiates a critical role of DAT in DA homeostasis in humans and highlights a potential contribution of disrupted DAT-function to pathophysiological conditions. Importantly, preclinical models ranging from flies (30) to mice (18,21) that express functionally penetrant, disease-associated coding variants of DAT provide an opportunity to examine the cellular and neurochemical underpinnings of DA-linked disorders.

In the current study, we utilized mice expressing DAT Val559 as a platform to search for a pharmacological manipulation that could normalize biochemical and behavioral traits seen with genetic DAT dysfunction. Specifically, based on considerations of the ability of the neuropeptide dynorphin, acting through KORs, to regulate presynaptic mechanisms in both nigrostriatal and mesolimbic DA neurons (87,88) and evidence that KOR antagonism offsets DAT-mediated changes *in vitro* and *in vivo* (our current study), we evaluated the potential of KOR blockade as a preclinical intervention to normalize neurochemical and behavioral changes arising in a construct valid model of DA dysfunction. We have shown that conversion of Ala559 to Val559 compromises the physiological function of WT DAT, producing spontaneous efflux of cytoplasmic DA (41,42), an effect found to be normalized by existing therapeutic DAT-targeting psychostimulants (41,42) *in vitro* as well as by antagonism of co-expressed D2 receptors (42). When expressed *in vivo*, DAT Val559 drives increased DAT surface expression in the DS but not in the VS of male mice (56), whereas, remarkably, this anatomical selectivity is opposite in female mice, occurring in the VS but not the DS (24). Behaviorally, mice expressing DAT Val559 present with perturbed behaviours, including, among others, abnormal locomotor reactivity (darting) on imminent handling (18), waiting

impulsivity and enhanced motivation for reward (19), and compulsive checking behavior in the presence of devalued reward (23). Underlying these traits, we have found that DAT Val559 mice display constitutive, presynaptic D2AR activation (18,56), blunted vesicular DA release (18,20) as well as blunted (amphetamine/methylphenidate) (18) or absent (cocaine) (24) locomotor responses to psychostimulants. In keeping with the sex and region-specific regulation of DAT by D2ARs (24,56), we detected differences in the neurochemical and behavioral phenotypes disrupted by DAT Val559 expression (24).

To offset the *in vivo* consequences of DAT Val559 expression, we reasoned that pharmacological strategies which directly prevent ADE (e.g. amphetamine or methylphenidate) or reduce the surface levels of efflux-prone transporters could offset DAT Val559 phenotypes. Previous efforts have shown that KOR and DAT exist as a physical complex, and that activation of KOR upregulates DAT function and surface expression (54). In combination with recently published clinical evidence demonstrating that KOR-antagonism is well-tolerated in humans (61–65), we explored whether antagonism of KOR-mediated regulation of DAT in our preclinical mouse model might support therapeutic potential for the treatment of DA-linked disorders.

We found that activation of KOR enhances DAT-mediated uptake by promoting an increase in surface DAT, consistent with a previous study (54), though the prior work did not explore the post-translational modifications and motif(s)/site(s) through which KOR regulates DAT surface expression. The intracellular domains of DAT serve as molecular hubs for interacting proteins and harbour consensus sites for various kinases (51,74). DAT exhibits constitutive phosphorylation *in vivo* (89), and ample evidence shows that both kinases and phosphatases regulate DAT expression, activity, and surface trafficking (51,73). The N-terminus of DAT contains phosphorylation sites that are modulated by PKC, ERK1/2, and CaMKII (74,90). Consistent with these findings, our current mutagenesis studies with heterologously-transfected cells revealed a requirement for an intact DAT N-terminus for KOR agonist stimulation of DAT surface trafficking. More specifically, whereas elevations comparable to WT DAT are evident in a truncated version of DAT that lacks the first 22 residues of the N-terminus, a larger truncation involving the first 55 N-terminal residues, completely eliminated KOR-mediated increases in DAT surface expression. Both D2ARs and KORs regulate DAT surface trafficking via an ERK1/2 dependent mechanism (52,54) and activation of D2ARs was found to promote enhanced surface trafficking and phosphorylation of DAT at Thr53 (56). Thus, we reasoned that KOR might enhance DAT surface trafficking and/or function by promoting enhanced phosphorylation of Thr53. Indeed, we found that mutation of the canonical ERK1/2 site Thr53 to Ala53 prevented the KOR agonist U69,593 from inducing elevations in DA transport V_{max},

DAT surface expression and phosphorylation of Thr53 DAT (Figures 1 and 2). In transient heterologous expression experiments, where distinct stages of biosynthetic progression are commonly observed (Figure 2), we observe a conspicuous loss of the mature glycosylated DAT isoform, suggesting an effect of the Thr53Ala substitution in transfected cells. This is indicative of a contribution of Thr53 or its phosphorylation to either progression through the biosynthetic pathway or stability of the mature transporter, which could therefore shape the V_{max} of DAT-mediated transport.

Enhanced DAT surface expression in acute brain slices, paralleled by elevated phosphorylation at Thr53, was evident in WT VS and DS slice preparations following KOR-agonist exposure. Moreover, high-speed chronoamperometry in live animals revealed that while the KOR-agonist U69,593 accelerated DA clearance, the KOR-antagonist norBNI prolonged DA clearance from the extracellular space, establishing for the first time the dependence of *in vivo* DA clearance on endogenous KOR signaling and consistent with a link of Thr53 phosphorylation to both KOR regulated trafficking and increased DA clearance capacity. Interestingly, we have previously demonstrated that D2AR-mediated regulation of DAT is sex and region specific, which results in elevated DAT Val559 surface expression and Thr53 hyperphosphorylation in the DS of males (56) and VS of females (24). In contrast, no region-specificity was observed for KOR in this regard (Figures 3 and 4). Of note, a recent report found that DAT-surface trafficking is sensitive to D2AR stimulation with the selective D2 agonist sumanirole in both the VS and DS, albeit with different kinetics evident in the VS and DS, with short-lived effects in the VS but sustained effects on surface trafficking seen in the DS (91). Interestingly, treatment with U69,593 significantly elevated surface DAT Val559 in the DS, without promoting a further increase in phosphorylation at Thr53 (Figure 4 E and F), which contrasts with our experiments in EM4 cells (Figure 2). This might indicate that phosphorylation at Thr53 reached a ceiling effect in the DS of DAT Val559 mice and that KOR can recruit additional and/or unknown regulatory mechanisms in native tissue preparations that are absent in heterologous expression systems. Using acute brain slices, we found that the KOR-antagonist norBNI remained without effect on DAT in the VS in terms of surface expression and phosphorylation (Figure 5 B and C). However, treatment with norBNI normalized the aberrant surface trafficking and hyperphosphorylation at Thr53 of DAT Val559 in the DS without affecting WT DAT (Figure 5 E and F). The increased phosphorylation and expression of efflux prone Val559 DAT presumably results from a tonic stimulation of D2ARs, as both phenotypes could be reversed with the D2 antagonist sulpiride (56). Our findings strongly support that inhibition of KOR normalizes the enhanced surface expression of DAT in the DS of male DAT Val559 mice.

Mergy and colleagues have shown that expression of DAT Val559 dampens the vesicular release of DA, due to tonic stimulation of inhibitory D2Ars (18). Consequently, administration of the non-selective DAT inhibitor cocaine, which restricts extracellular DA levels to that achieved by excitation-induced vesicular DA release, fails elevate extracellular DA in the DS of male Val559 mice as measured by microdialysis (20). We found that pre-treatment with norBNI fully restored the response to cocaine in male mice. This finding supports the interpretation that inhibition of KOR and subsequent normalization of surface trafficking of DAT Val559 aids in restoration of vesicular DA release in DAT Val559 mice. Additional studies are needed to clarify the contribution of somatic KOR versus presynaptic KOR in the ability of KOR antagonists to restore vesicular DA despite elevated D2AR signaling. Mice are available that lack KOR in DAergic neurons (92). Future studies with such animals should help define whether the effect of norBNI in DAT Val559 mice exclusively relies on its action at KORs expressed on DA synthesizing neurons versus other sites. Similarly, additional approaches are needed to identify the source(s) of dynorphin that allow for the ability of KOR to normalize traits in DAT Val559 mice. While a striatal source of dynorphin that could account for modulation of DAT Val559 by transporter regulating KORs has been documented (12), we have demonstrated that a serotonergic plasticity arises in DAT Val559 mice that drives a loss of locomotor activation by cocaine . In this regard, Pomrenze et al (93) have recently demonstrated that serotonergic projections to the NAc produce and release dynorphin and are worth exploring.

At present, we cannot exclude the possibility that treatment with norBNI reduces DAT Val559-mediated reverse transport *per se* as well as surface expression. DAT Val559 is hyperphosphorylated at DAT N-terminal sites that have been linked to reverse transport (42,66). Antagonism of KOR normalized the hyperphosphorylation at Thr53 and this observation could expand to other phosphorylation sites crucial for reverse transport. Further, Lycas et al (94) reported that activation of D2ARs causes DAT to accumulate in nanoclusters in which DAT appears to be biased towards the inward facing conformation. The authors found that another efflux-prone DAT variant (DAT-Asp421Asn) that is conformationally biased towards the inward-facing conformation preferentially localized to these clusters. Considering the tonic activation of D2ARs, DAT Val559 may indeed reside in nanodomains that support ADE in DAergic neurons whereas antagonism of KOR could redistribute DAT Val559 into nano-environments that preclude ADE. Alternatively, antagonism of KOR could further disrupt the potentially enhanced interaction of DAT Val559 with proteins and lipids that bias DAT towards more efflux-prone states (49,95–98). Activated Gbg proteins have also been found to induce DA efflux similar to that seen with DAT Val559 and amphetamines (44,45). Whether the pathways involved with KOR antagonism intersect with this mechanism and its

regulators are worthy of study. More generally, such considerations suggest that DAT mutations are likely only one mechanism by which behaviorally penetrant DA efflux states can arise, and where KOR antagonism can be of therapeutic use.

On a behavioral level, male DAT Val559 mice display a deficit in spontaneous alternation in the Y-Maze test (Stewart 2022 and Figure 7), which translates into deficits in working memory (Lalonde 2007-11835987). We found no difference in locomotor activity during Y maze tests, which argues against the interpretation that the differences in alternations result from a hyper- or hypoactive phenotype (Figure 7 and Stewart 2022). Importantly, administration of norBNI normalized the deficit in spontaneous alternations and direct revisits 30 min and one week post injection. The latter observation is consistent with the long-lasting effects of norBNI (70,71). The frontal cortex has been prominently associated with behaviors assessed in the Y-Maze, including working memory, spatial learning and cognition (99). Deficits in extracellular DA in the medial prefrontal cortex (mPFC) were found to be linked to a reduction in spontaneous alternations (100). In rats, lesions to the NAc lacked effect on spontaneous alternations (101,102), whereas lesions to the VTA resulted in a robust deficit in alternations (103). These findings suggest that DAT Val559 expression could alter mesocortical DAergic projections in male mice and warrants further investigation on the impact of ADE on mesolimbic versus mesocortical pathways. It is also possible that the deficit in spontaneous alternations observed with DAT Val559 in the Y-Maze could be attributed to DAT Val559-associated alterations in the DS, as lesions to the dorsomedial striatum were found to affect spatial cognition in mice (104). Hence, studies assessing DA dynamics in WT and DAT Val559 in mPFC, VS and DS in the context of DAT, D2AR and KOR antagonists directly administered in these regions are needed to tease apart the relative contribution of the respective terminal fields of DA neurons emanating from VTA and SNc.

In line with the persistent effect of norBNI in the Y-Maze, we also found that norBNI normalized behavior of male Val559 mice in the open field one week after norBNI administration, consistent with an anxiolytic effect. When treated with vehicle, DAT Val559 mice spent significantly less time in the center than WT controls and this difference was absent when mice were treated with norBNI prior to testing (Figure 8). Interestingly, we (18) found no differences in horizontal locomotor activity between WT and DAT Val559 mice in the open field. The reduction in horizontal locomotor activity of male Val559 DAT mice observed in this study might be attributed to repeated handling of the mice and an increased susceptibility of these mice to repeated stress. We also observed that saline treated DAT Val559 mice displayed a reduced

tendency to explore the full length of the arms of the Y-Maze when they were re-exposed to the apparatus. This could indicate that the exploratory behaviour is suppressed in male DAT Val559 upon repeated handling or when the novelty of the environment is removed. Moreover, pre-treatment with norBNI restored the locomotor response of male DAT Val559 mice to systemic cocaine in the open field, indicative of re-established vesicular DA release in norBNI treated DAT Val559 mice. Finally, we have recently reported that female DAT Val559 mice display impaired performance in NOR task and that this phenotype can be restored by systemic administration of the D2-antagonist sulpiride (24), in line with our interpretation that behavioral deficits arise from tonic activation of D2ARs. Systemic administration of norBNI improved NOR in female DAT Val559 mice, which suggests that antagonism of KOR rescues behavioral consequences of DAT Val559 expression regardless of sex.

Our findings support the use of a non-stimulant type medication for the treatment of DA-linked disorders that manifest in a reduction in cognitive function and/or working memory. Consistent with this idea, a recent study demonstrated that norBNI improved working memory and attention in a perinatal nicotine exposure model (100). The authors concluded that this effect arises from an increase in cortical DA following administration of norBNI. Prenatal exposure to nicotine alters development of the DA system and direct effects of this paradigm on DAT have been reported (105). Moreover, nicotinic acetylcholine receptors are well known to regulate DA vesicular release (106). This suggests that the beneficial effect of norBNI could arise from normalization of disrupted presynaptic signaling networks that dictate DA release and clearance.

In conclusion, using a construct-valid preclinical model of genetic DAT dysfunction, we found that inhibition of KOR normalizes aberrant biochemical and behavioral sequelae resulting from disrupted DAergic neurotransmission, reinforcing the potential of KOR antagonists for the treatment of disorders linked to DAT-dependent tonic DA elevation. Additionally, our findings draw attention to the interplay of D2AR and KOR signaling and their regulation of DAT and DA neurotransmission under basal conditions, as well augmentating vesicular DA release to achieve greater neuromodulatory DA “signal to noise”. Considering issues of high abuse liability with prescribing psychostimulants to treat many DA-linked psychiatric pathologies, our findings offer a salient example of how converging signaling pathways can be targeting to normalize DA signaling *in vivo*.

Acknowledgements

This work was supported by a Max Kade Fellowship of the Austrian Academy of Sciences to FPM, a NARSAD Young Investigator Grant from the BBRF to AS, P20 GM103442 to JDF, P20 GM104360 to RAV, R01 MH093320 and R21 DA046044 to LCD, R01 MH105094 to RDB and R01DA054694 to SR

Figure 1

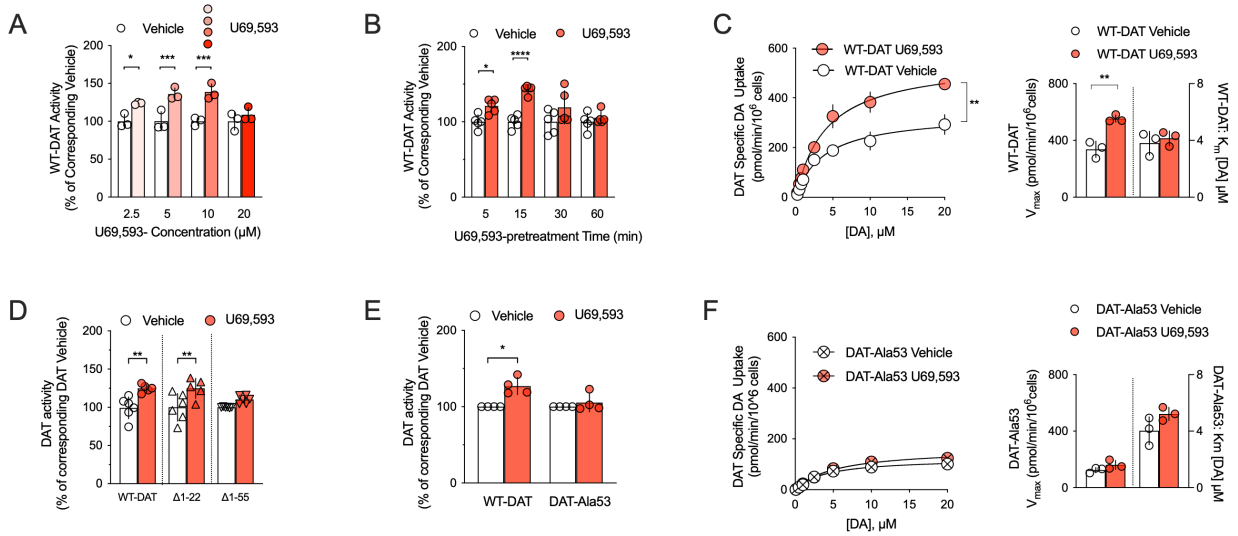

Figure 1: The KOR agonist U69,593 increases DAT-mediated uptake via a Thr53 dependent mechanism. EM4 cells were transfected with DAT and KOR and uptake of [^{3}H]DA was assessed as described in Methods.

A: U69,593 (10 µM) increased WT DAT-mediated uptake in rDAT/rKOR cotransfected EM4 cells in a concentration-dependent manner as compared to vehicle (n= 3 independent observations per condition, one-way ANOVA, followed by Bonferroni post-hoc tests).

B: Treatment with 10 µM U69,593 enhanced WT DAT specific uptake in a time-dependent fashion (n= 5 independent observations per condition, one-way ANOVA, followed by Bonferroni post-hoc tests).

C: Incubation with 10 µM U69,593 increased WT DAT V_{max} (two-tailed unpaired t-test) without effect on K_M (n=3 independent observations per condition, two-tailed Student's unpaired t-test).

D: Treatment with U69,593 significantly augmented WT DAT-mediated uptake when compared to vehicle in cells that expressed KOR plus either WT DAT or a truncated version of DAT, lacking the first 22 N-terminal residues (DAT Δ1-22). In contrast, truncation of the first 55 N-terminal residues (DAT Δ1-55 DAT) prevented KOR-agonist induced increases in [^{3}H]DA uptake. (n=5-6 independent observations per condition, one-way ANOVA, followed by Bonferroni post-hoc tests)

E: Site-directed mutagenesis of DAT Thr53 to alanine (DAT-Ala53) rendered transporter-mediated DA uptake insensitive to pre-treatment with U69,593 at 5 and 10 µM (n=4 observations per condition, One-way ANOVA, followed by Bonferroni posthoc tests).

F: U69,593 did not affect the kinetic parameters K_M and V_{max} of the DAT-Ala53 mutant (n=3 independent observations per condition, Student's two-tailed unpaired t-test)

Data are shown as the mean with error bars reflecting the SD *=P<0.05; **=P<0.01; ***=P<0.001; ****=P<0.0001.

Figure 2

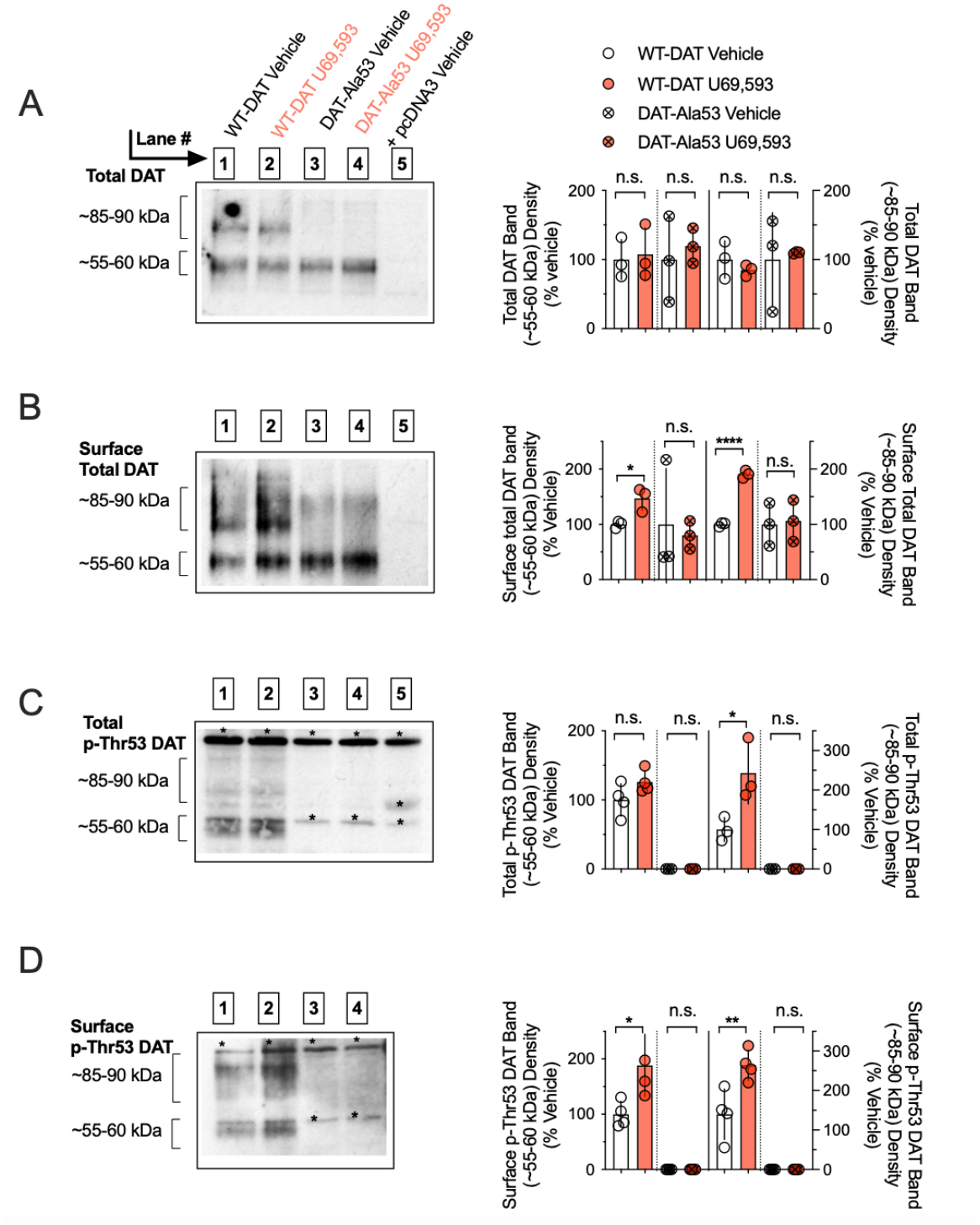

Figure 2: Capacity to phosphorylate rDAT at Thr53 is required for rKOR activation to elevate transporter surface expression

EM4 cells were transfected with either WT DAT or DAT Ala53 plus rKOR, subjected to U69,593 and biotinylated as described in Methods.

A: Treatment with U69,593 did not affect WT DAT band densities at ~55-60 kDa and ~85-90 kDa, derived from total protein lysates (n=3 independent observations per condition, Student's two-tailed unpaired t-test).
B: Incubation with U69,593 increased the WT DAT band densities at ~55-60 kDa and ~85-90 kDa, derived from biotinylated protein lysates (unpaired, two-tailed t-test). No effect was observed on the DAT Ala53 band densities at ~55-60 kDa (n=3 independent observations per condition, Student's two-tailed unpaired t-test).
C and D: Protein lysates were immunoblotted with p-Thr53 antibody. Bands marked with an asterisk indicate non-specific immunoreactivity.
C: In total protein lysates, incubation with U69,593 increased the density of the p-Thr53 immunoreactive band at ~55-60 kDa for WT DAT (Student's unpaired, two-tailed t-test). No effect was observed on the band densities at ~85-90 kDa. No specific bands were detected for the DAT Ala53 variant (n=3-5 independent observations per condition, Student's two-tailed unpaired t-test).
D: U69,593 augmented band densities at ~55-60 and ~85-90 kDa for biotinylated WT DAT (n=5 independent observations per condition, Student's two-tailed unpaired t-test). No specific bands were detected for the DAT Ala53 variant.
All bars represent the mean with error bars reflecting the SD. Individual quantifications are displayed as individual symbols. *=P<0.05; **=P<0.01; ****=P<0.0001. n.s.=not significant

Figure 3

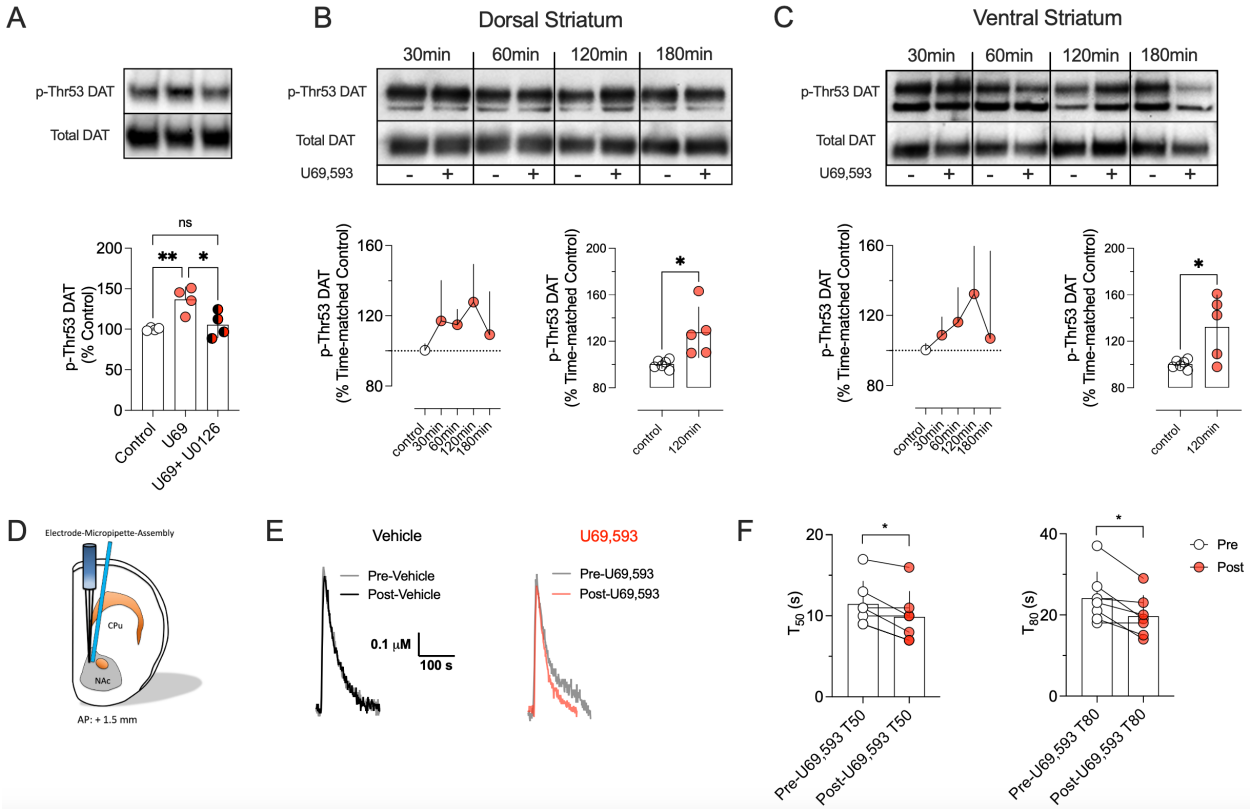

Figure 3: KOR-agonism enhances phosphorylation of DAT at Thr53 in native preparations and augments DAT-mediated clearance in the NAc *in vivo*.

A) Male rat striatal synaptosomes were treated with vehicle or 50 µM U0126 for 15 min at 30˚C, followed by treatment with vehicle or 10 µM U69,593 for an additional 15 min 30˚C. After treatment, samples were subjected to SDS-PAGE and western blotted for total and p-Thr53 DAT. Upper panel shows representative western blots. Lower panel shows quantification of p-Thr53 DAT staining as a percentage of basal levels. (n=4; one-way ANOVA, Tukey's multiple comparisons test).

B and C) Rats were injected s.c. with vehicle or U69,593 (0.32 mg/kg) and sacrificed at indicated times. Tissue from the dorsal **(B)** or ventral striatum **(C)** were western blotted for total and p-Thr53 DAT in duplicate. Signals from the U69,593 treated samples were compared to the time-matched control. The upper panels show representative western blots for the dorsal and ventral striatum with each time-matched control followed by U69,593 treatment. The lower panels show quantification of the p-Thr53 DAT staining as a percentage of the time-matched control (Two-tailed, unpaired t-test).

D) Schematic representation of the electrode-micropipette assembly that was lowered into the NAc of anaesthetized rats to allow for *in vivo* chromatographic measurement of DA clearance rates.

E) Representative oxidation currents converted to micromolar values observed upon pressure ejection of DA before (gray traces) and 2 min after intra-NAc injection of vehicle (black trace), U69,593 (890 µM, barrel concentration, red trace). The leftward-shift in the representative trace following U69,593 injection is indicative of increased DA clearance.

F) U69,593 decreased the clearance time of exogenously applied DA in the NAc (T_{50} and T_{80}; n= 7 observations per condition, two-tailed paired t-test) when compared to the pre-drug value. Bars indicate the mean and error reflect SD. Individual values from each animal are reflected by the corresponding symbols. *denotes P<0.05; **denotes P<0.01, ns = not significant.

Figure 4

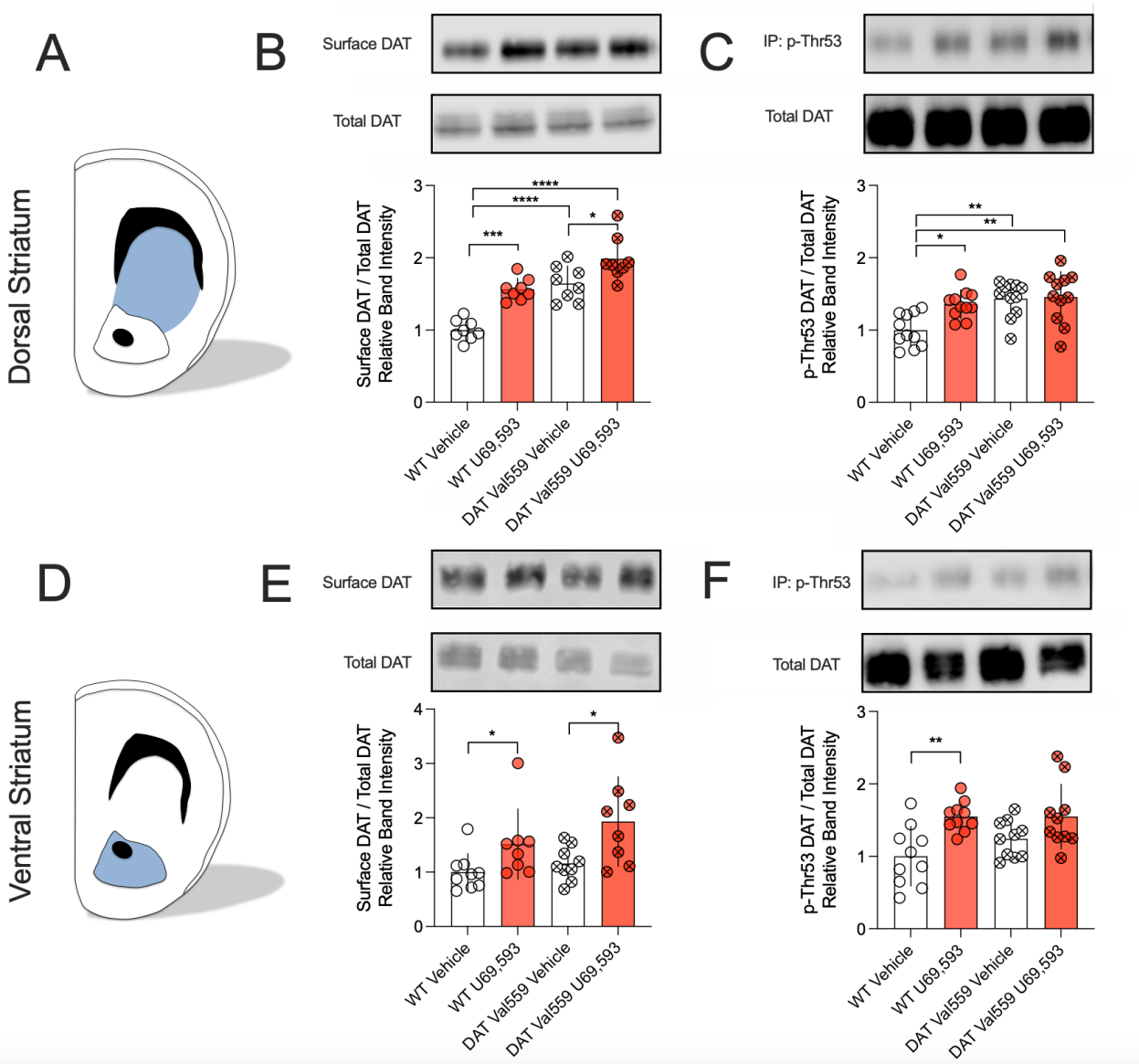

Figure 4: mKOR agonism induces enhanced mDAT surface expression and phosphorylation at mDAT Thr53 in acute brain slices containing the DS or VS .

Acute slices containing the DS (highlighted in area in A) and/or the VS (highlighted area in D) were exposed to 10 µM of U69,693 or vehicle for 7 min and surface expression and phosphorylation of p-Thr53 DAT was assessed as described in Methods.

B and C) In the DS, treatment with U69,593 increased surface DAT levels (B) (n=9; two-way ANOVA, Šídák's multiple comparisons test) as well as phosphorylation of mDAT at Thr53 (C) (n=10; two-way ANOVA, Šídák's multiple comparisons test).

E) In the VS, KOR-agonist treatment increased surface mDAT levels independent of genotype as compared to vehicle treatment (n=8; two-way ANOVA, Šídák's multiple comparisons test).

F) Treatment with U69,593 enhanced WT mDAT phosphorylation at Thr53, but remained without effect on DAT Val559 phosphorylation. Higher basal phosphorylation levels at Thr53 were detected for the DAT Val559 when compared to WT DAT in the DS (n=11; two-way ANOVA, Šídák's multiple comparisons test).

All bars show the mean and SD. Symbols reflect individual observations. * = $P \leq 0.05$, ** = $P \leq 0.01$, *** = $P \leq 0.001$, **** = $P \leq 0.0001$.

Figure 5

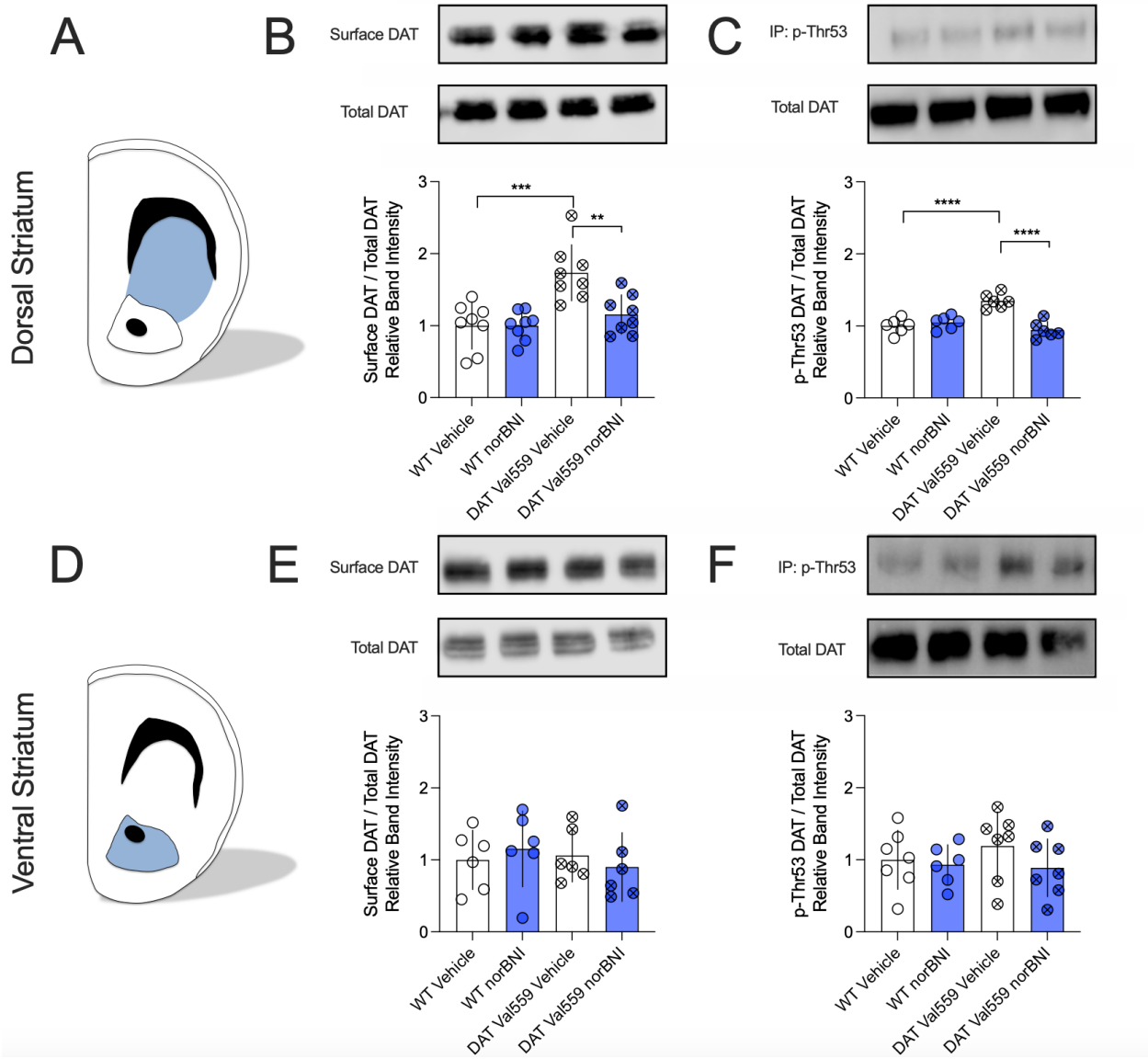

Figure 5: mKOR antagonism reduces the elevated surface expression and Thr53 phosphorylation of DAT Val559 in the DS without affecting WT DAT in acute slices and with no effects in the VS.
Acute coronal slices containing the DS (highlighted in area in A) or the VS (highlighted in area in **D)** were treated with the KOR antagonist norBNI (1 µM) for 20 min and DAT surface expression and phosphorylation at Thr53 were determined as described in Methods.
B and **C)** In the DS, antagonism of mKOR reduced the enhanced surface expression **(B)** (n=8; two-way ANOVA, Šídák's multiple comparisons test) and Thr-53 phosphorylation **(C)** (n=6; two-way ANOVA, Šídák's multiple comparisons test) of tansporters in DAT Val559 mice. No effect was detected with WT DAT mice.
E and **F)** Treatment with norBNI remained without effect on DAT surface expression **(E)** (n=6, two-way ANOVA, Šídák's multiple comparisons test) and Thr-53 phosphorylation **(F)** (n= 7, two-way ANOVA, Šídák's multiple comparisons test) in the VS.
All bars show the mean and SD. Symbols reflect individual observations. ** = $P \leq 0.01$, *** = $P \leq 0.001$, **** = $P \leq 0.0001$

Figure 6

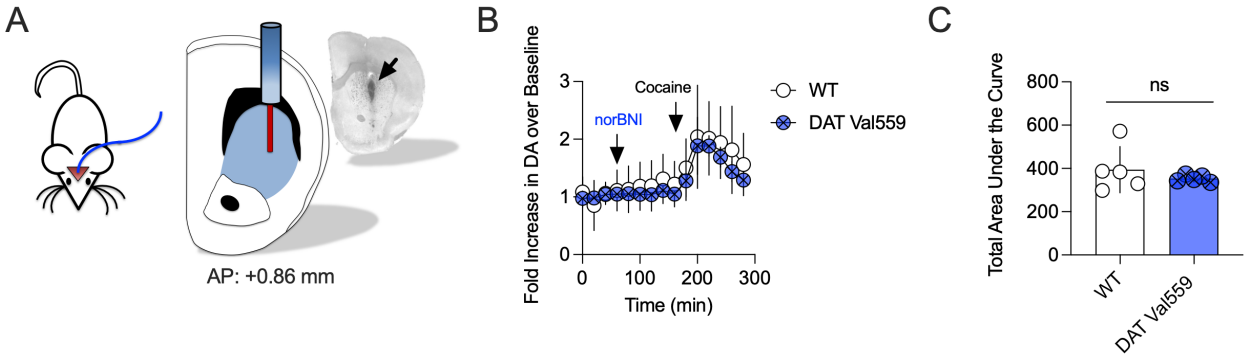

Figure 6: Pretreatment with norBNI restores cocaine-induced increase in extracellular DA the DS of freely moving DAT Val559 mice

A) Cartoon displaying the placement of the microdialysis probe in the DS. The insert shows a coronal slice with the black the arrow indicating the position of the active dialysis probe.

B) Male WT and DAT Val559 mice were injected with norBNI (10 mg/kg, i.p.) and cocaine (10 mg/kg, i.p.) and extracellular DA was measured using *in vivo* microdialysis in the DS.

20 min samples where collected and DA is expressed as fold increase of basal DA (i.e. the average from t=0 to 60 min). Arrows indicate times for systemic administration of norBNI and cocaine. N=5 animals per genotype, data are shown as mean and SD.

C) Shown is the total area under the curve for the traces shown in **(B)**. Data are shown as the mean and error bars indicate the SD. Ns= not significant, unpaired Student's t-test with Welch's correction.

Figure 7

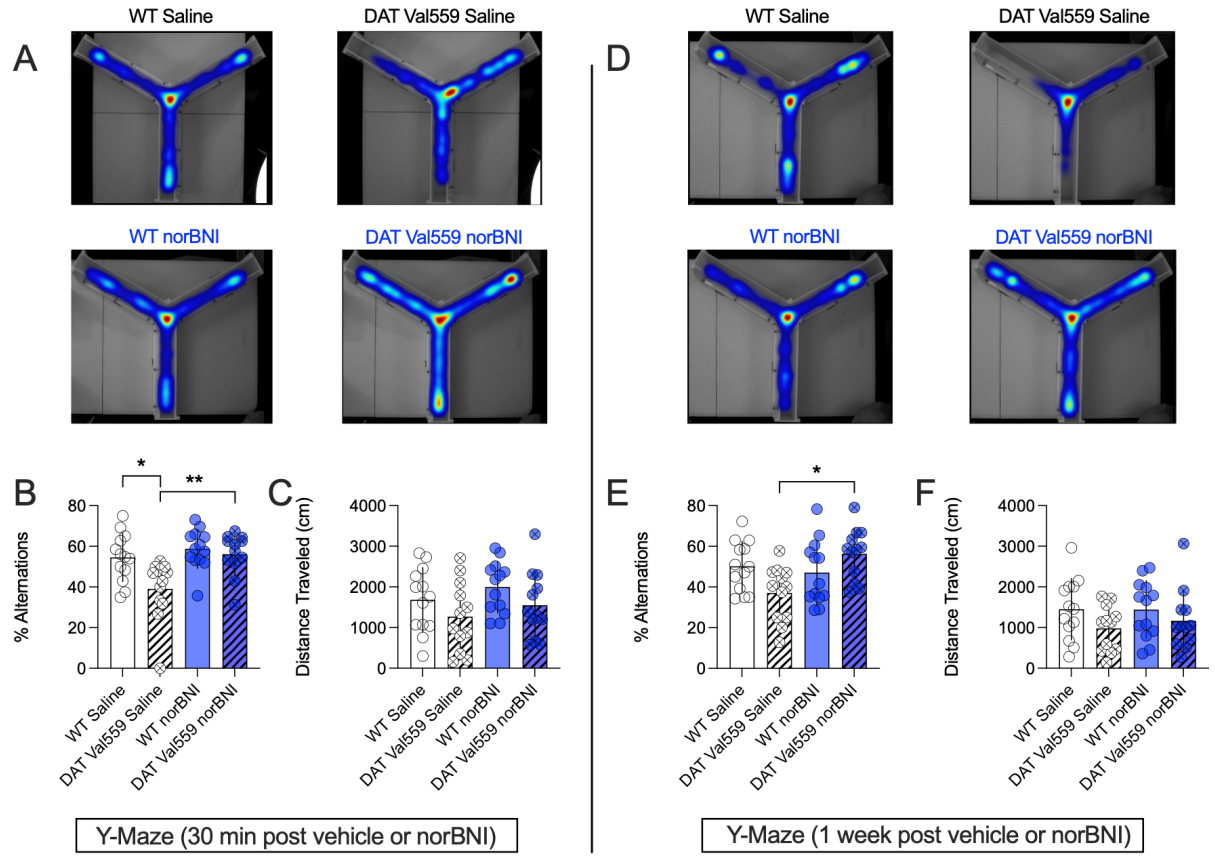

Figure 7: Treatment with norBNI normalizes the spontaneous alternation deficit of male Val559 DAT mice in the Y-maze test

Male homozygous DAT Val559 mice and their WT littermates were injected with saline (vehicle) or norBNI (10 mg / kg, i.p.) and placed into the center of the open maze and the number of alternating arm entries and distance travelled were recorded as described in Methods.

A) Representative heat maps showing the explorative behavior of WT and Val559 mice following vehicle or norBNI administration (30 min). Time spent in each area is directly correlated to the color gradient ranging from dark blue to dark red, with the latter indicating highest value.

B) Systemic administration of norBNI 30 min prior to the test normalized the deficit in the percentage of alternations of DAT Val559 DAT mice when compared to WT control mice.

C) No acute effect of norBNI was observed for total distance travelled during the test session.

D) The same cohort of mice shown in A-C was retested in the Y-Maze one week after the administration of norBNI with representative heat maps shown as in in A)

E**)** DAT Val559 mice treated with vehicle displayed significantly fewer alternations when compared to DAT Val559 injected with norBNI.

F) No differences between genotypes or drug treatment groups on total distance travelled were detected one week after norBNI administration.

All bars show the mean and SD. n=12-13 individual animals per group, data in A through E were analyzed with two-way ANOVA, Šídák's multiple comparisons test. Symbols reflect individual animals. * = $P \leq 0.05$, ** = $P \leq 0.01$, ns = not significant.

Figure 8

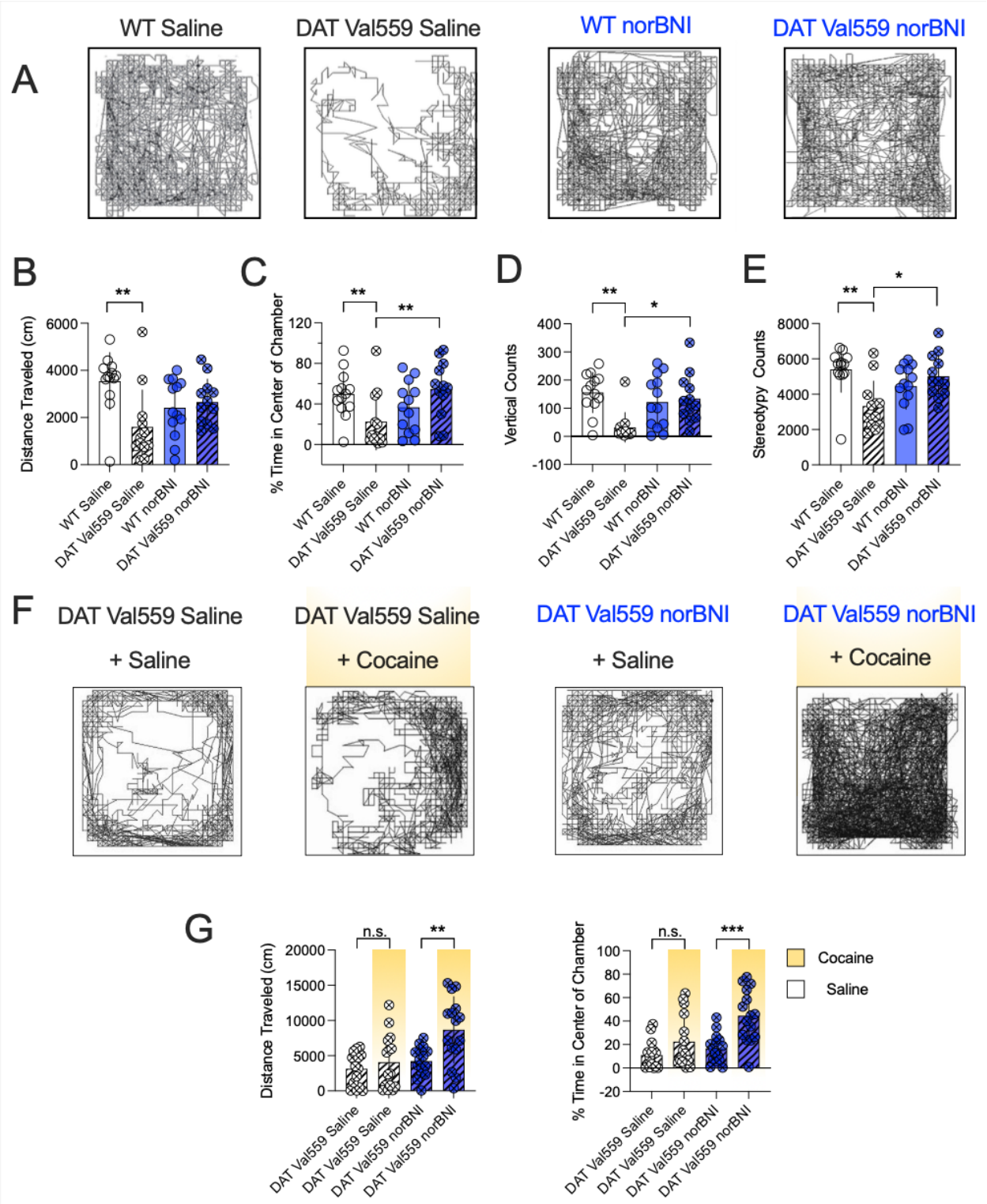

Figure 8 norBNI treatment of male DAT Val559 mice normalizes abnormal locomotor responses to injection stress and locomotor response to systemic cocaine as monitored in the open field test

A-E) Homozygous male DAT Val559 and WT littermates were injected with saline (vehicle) or norBNI (10 mg/kg, i.p.) and placed in open activity chambers one week post injection.

A) Representative activity traces of WT and DAT Val559 mice. DAT Val559 mice previously injected with vehicle (saline) displayed significantly less B) forward locomotor activity C) spent less time in the center of the activity chamber and exhibited fewer
D) vertical counts and E) stereotypies when compared to WT mice. No differences between genotypes were detected when the mice were pretreated with norBNI.
F-G) Homozygous male DAT Val559 were injected with saline or cocaine (10 mg/kg, i.p.) one week post administration of norBNI (10 mg/kg, i.p.) and placed into open activity chambers.
F) Representative traces of male DAT Val559 mice injected with the indicated drug combinations. G) Total distance travelled and time spent in the center of the chamber of male DAT Val559 mice injected with the indicated combinations of saline, norBNI and cocaine.
All bars show the mean and SD. n=12-13 individual animals per group, data in B, C, D, E and G were analyzed with two-way ANOVA, Šídák's multiple comparisons test. Symbols reflect individual animals. * = $P \leq 0.05$, ** = $P \leq 0.01$, *** = $P \leq 0.001$, ns = not significant.

Figure 9

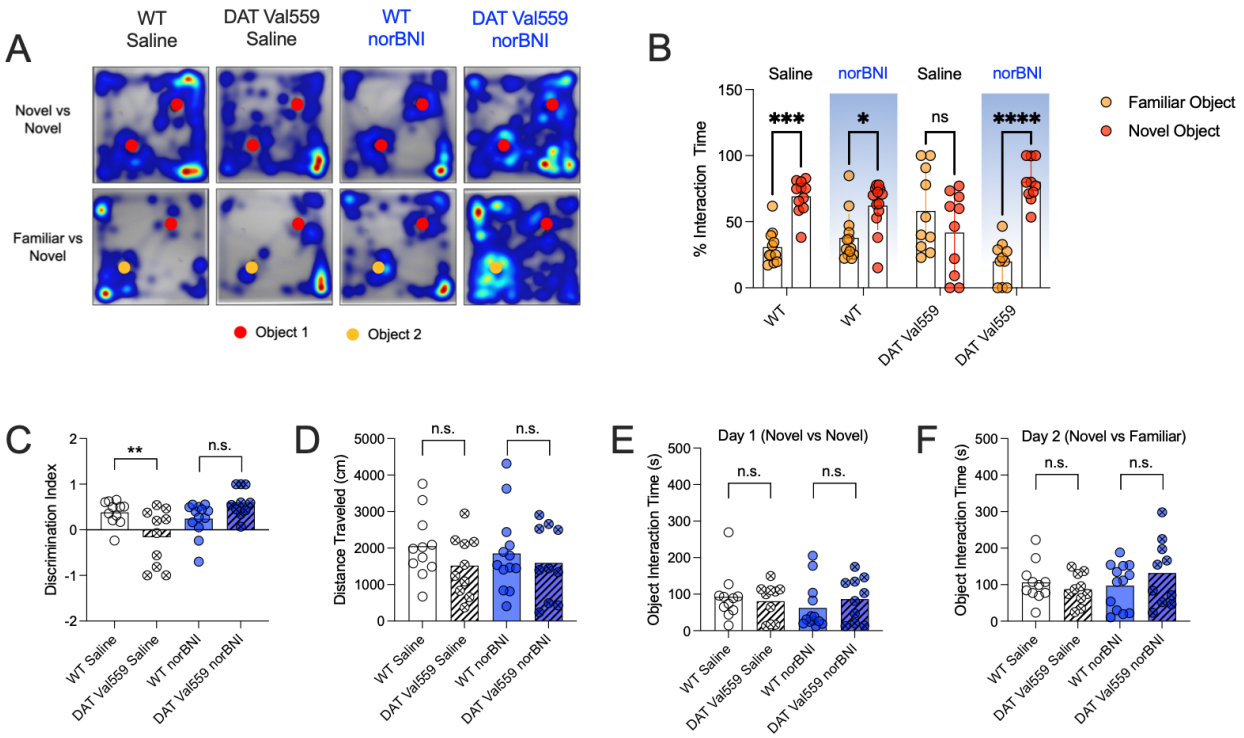

Figure 9: Pretreatment with norBNI renders the phenotype of female DAT Val599 mice in the novel object recognition task comparable to female WT mice. The NOR task was performed with saline treated female WT (n=11) and DAT Val559 littermates (n=10) and compared to norBNI treated (10 mg/kg, i.p., 30 min prior to testing) female WT (n=13) and littermate DAT Val559 (n=10) mice.
A) provides representative heat maps representing location in relation to objects (circles) used in NOR sessions. The relative interaction time with the familiar versus the novel object and the discrimination index are shown in (B) and (C), respectively.
D) shows the total distance travelled and the total object interaction times on day 1 (two novel objects) and day 2 (one novel and one familiar object) are shown in panels (E) and (F), respectively. Data are given as mean and SD and were analyzed using two-way ANOVA with Šídák's multiple comparisons test. *=P<0.05, **=P<0.01, ***=P<0.001, ****=P<0.0001, n.s.= not significant.

References

1. Bromberg-Martin ES, Matsumoto M, Hikosaka O. Dopamine in Motivational Control: Rewarding, Aversive, and Alerting. Vol. 68, Neuron. 2010. p. 815–34.
2. Berke JD. What does dopamine mean? Vol. 21, Nature Neuroscience. Nature Publishing Group; 2018. p. 787–93.
3. Salamone JD. Complex motor and sensorimotor functions of striatal and accumbens dopamine: involvement in instrumental behavior processes. Vol. 107, Psychopharmacology. 1992.
4. Barnes JJM, Dean AJ, Nandam LS, O'Connell RG, Bellgrove MA. The molecular genetics of executive function: role of monoamine system genes. Biol Psychiatry. 2011 Jun 15;69(12):e127-43.
5. Volkow ND, Wang GJ, Kollins SH, Wigal TL, Newcorn JH, Telang F, et al. Evaluating Dopamine Reward Pathway in ADHD Clinical Implications [Internet]. 2009. Available from: https://jamanetwork.com/
6. Pavăl D. A Dopamine Hypothesis of Autism Spectrum Disorder. Dev Neurosci. 2017;39(5):355–60.
7. Ashok AH, Marques TR, Jauhar S, Nour MM, Goodwin GM, Young AH, et al. The dopamine hypothesis of bipolar affective disorder: the state of the art and implications for treatment. Mol Psychiatry. 2017 May;22(5):666–79.
8. Dauer W, Przedborski S. Parkinson's disease: mechanisms and models. Neuron. 2003 Sep 11;39(6):889–909.
9. Grace AA. Dysregulation of the dopamine system in the pathophysiology of schizophrenia and depression. Nat Rev Neurosci. 2016 Aug;17(8):524–32.
10. Russo SJ, Nestler EJ. The brain reward circuitry in mood disorders. Nat Rev Neurosci. 2013 Sep;14(9):609–25.
11. Kristensen AS, Andersen J, Jørgensen TN, Sørensen L, Eriksen J, Loland CJ, et al. SLC6 neurotransmitter transporters: structure, function, and regulation. Pharmacol Rev. 2011 Sep;63(3):585–640.
12. Giros B, Jaber M, Jones SR, Wightman RM, Caron MG. Hyperlocomotion and indifference to cocaine and amphetamine in mice lacking the dopamine transporter. Nature. 1996 Feb 15;379(6566):606–12.
13. Jones SR, Gainetdinov RR, Jaber M, Giros B, Wightman RM, Caron MG. Profound neuronal plasticity in response to inactivation of the dopamine transporter. Proc Natl Acad Sci U S A. 1998 Mar 31;95(7):4029–34.
14. Madras BK, Miller GM, Fischman AJ. The Dopamine Transporter and Attention-Deficit/Hyperactivity Disorder. Biol Psychiatry. 2005 Jun;57(11):1397–409.
15. Pinsonneault JK, Han DD, Burdick KE, Kataki M, Bertolino A, Malhotra AK, et al. Dopamine transporter gene variant affecting expression in human brain is associated with bipolar disorder. Neuropsychopharmacology. 2011 Jul;36(8):1644–55.
16. Heal DJ, Smith SL, Gosden J, Nutt DJ. Amphetamine, past and present--a pharmacological and clinical perspective. J Psychopharmacol. 2013 Jun;27(6):479–96.
17. Volkow ND, Wang GJ, Fowler JS, Logan J, Franceschi D, Maynard L, et al. Relationship between blockade of dopamine transporters by oral methylphenidate and the increases in extracellular dopamine: therapeutic implications. Synapse. 2002 Mar 1;43(3):181–7.
18. Mergy MA, Gowrishankar R, Gresch PJ, Gantz SC, Williams J, Davis GL, et al. The rare DAT coding variant Val559 perturbs da neuron function, changes behavior, and alters in vivo responses to psychostimulants. Proc Natl Acad Sci U S A. 2014 Nov 4;111(44):E4779–88.
19. Davis GL, Stewart A, Stanwood GD, Gowrishankar R, Hahn MK, Blakely RD. Functional coding variation in the presynaptic dopamine transporter associated with neuropsychiatric disorders

drives enhanced motivation and context-dependent impulsivity in mice. Behavioural brain research. 2018 Jan 30;337:61–9.
20. Stewart A, Davis GL, Gresch PJ, Katamish RM, Peart R, Rabil MJ, et al. Serotonin transporter inhibition and 5-HT2C receptor activation drive loss of cocaine-induced locomotor activation in DAT Val559 mice. Neuropsychopharmacology. 2019 Apr;44(5):994–1006.
21. DiCarlo GE, Aguilar JI, Matthies HJ, Harrison FE, Bundschuh KE, West A, et al. Autism-linked dopamine transporter mutation alters striatal dopamine neurotransmission and dopamine-dependent behaviors. J Clin Invest. 2019 May 16;129(8):3407–19.
22. Ragu Varman D, Subler MA, Windle JJ, Jayanthi LD, Ramamoorthy S. Novelty-induced hyperactivity and suppressed cocaine induced locomotor activation in mice lacking threonine 53 phosphorylation of dopamine transporter. Behavioural brain research. 2021 Jun 25;408:113267.
23. Stewart A, Davis GL, Areal LB, Rabil MJ, Tran V, Mayer FP, et al. Male DAT Val559 Mice Exhibit Compulsive Behavior under Devalued Reward Conditions Accompanied by Cellular and Pharmacological Changes. Cells. 2022 Dec 15;11(24).
24. Stewart A, Mayer FP, Gowrishankar R, Davis GL, Areal LB, Gresch PJ, et al. Behaviorally penetrant, anomalous dopamine efflux exposes sex and circuit dependent regulation of dopamine transporters. Mol Psychiatry. 2022 Dec;27(12):4869–80.
25. Reith MEA, Kortagere S, Wiers CE, Sun H, Kurian MA, Galli A, et al. The dopamine transporter gene SLC6A3: multidisease risks. Mol Psychiatry. 2022 Feb;27(2):1031–46.
26. Mazei-Robison MS, Couch RS, Shelton RC, Stein MA, Blakely RD. Sequence variation in the human dopamine transporter gene in children with attention deficit hyperactivity disorder. Neuropharmacology. 2005 Nov;49(6):724–36.
27. Sakrikar D, Mazei-Robison MS, Mergy MA, Richtand NW, Han Q, Hamilton PJ, et al. Attention deficit/hyperactivity disorder-derived coding variation in the dopamine transporter disrupts microdomain targeting and trafficking regulation. J Neurosci. 2012 Apr 18;32(16):5385–97.
28. Hansen FH, Skjørringe T, Yasmeen S, Arends N V, Sahai MA, Erreger K, et al. Missense dopamine transporter mutations associate with adult parkinsonism and ADHD. J Clin Invest. 2014 Jul;124(7):3107–20.
29. Grünhage F, Schulze TG, Müller DJ, Lanczik M, Franzek E, Albus M, et al. Systematic screening for DNA sequence variation in the coding region of the human dopamine transporter gene (DAT1). Mol Psychiatry. 2000 May;5(3):275–82.
30. Hamilton PJ, Campbell NG, Sharma S, Erreger K, Herborg Hansen F, Saunders C, et al. De novo mutation in the dopamine transporter gene associates dopamine dysfunction with autism spectrum disorder. Mol Psychiatry. 2013 Dec;18(12):1315–23.
31. de Azeredo LA, Rovaris DL, Mota NR, Polina ER, Marques FZ, Contini V, et al. Further evidence for the association between a polymorphism in the promoter region of SLC6A3/DAT1 and ADHD: findings from a sample of adults. Eur Arch Psychiatry Clin Neurosci. 2014 Aug;264(5):401–8.
32. Bowton E, Saunders C, Reddy IA, Campbell NG, Hamilton PJ, Henry LK, et al. SLC6A3 coding variant Ala559Val found in two autism probands alters dopamine transporter function and trafficking. Transl Psychiatry. 2014 Oct 14;4(10):e464.
33. Mazei-Robison MS, Blakely RD. Expression studies of naturally occurring human dopamine transporter variants identifies a novel state of transporter inactivation associated with Val382Ala. Neuropharmacology. 2005 Nov;49(6):737–49.
34. Herborg F, Andreassen TF, Berlin F, Loland CJ, Gether U. Neuropsychiatric disease-associated genetic variants of the dopamine transporter display heterogeneous molecular phenotypes. J Biol Chem. 2018 May 11;293(19):7250–62.

35. Bhat S, El-Kasaby A, Freissmuth M, Sucic S. Functional and Biochemical Consequences of Disease Variants in Neurotransmitter Transporters: A Special Emphasis on Folding and Trafficking Deficits. Pharmacol Ther. 2021 Jun;222:107785.
36. Leitner Y. The co-occurrence of autism and attention deficit hyperactivity disorder in children - what do we know? Front Hum Neurosci. 2014;8:268.
37. Rommelse NNJ, Franke B, Geurts HM, Hartman CA, Buitelaar JK. Shared heritability of attention-deficit/hyperactivity disorder and autism spectrum disorder. Eur Child Adolesc Psychiatry. 2010 Mar;19(3):281–95.
38. Zhou A, Cao X, Mahaganapathy V, Azaro M, Gwin C, Wilson S, et al. Common genetic risk factors in ASD and ADHD co-occurring families. Hum Genet. 2023 Feb;142(2):217–30.
39. Schiweck C, Arteaga-Henriquez G, Aichholzer M, Edwin Thanarajah S, Vargas-Cáceres S, Matura S, et al. Comorbidity of ADHD and adult bipolar disorder: A systematic review and meta-analysis. Neurosci Biobehav Rev. 2021 May;124:100–23.
40. van Hulzen KJE, Scholz CJ, Franke B, Ripke S, Klein M, McQuillin A, et al. Genetic Overlap Between Attention-Deficit/Hyperactivity Disorder and Bipolar Disorder: Evidence From Genome-wide Association Study Meta-analysis. Biol Psychiatry. 2017 Nov 1;82(9):634–41.
41. Mazei-Robison MS, Bowton E, Holy M, Schmudermaier M, Freissmuth M, Sitte HH, et al. Anomalous dopamine release associated with a human dopamine transporter coding variant. J Neurosci. 2008 Jul 9;28(28):7040–6.
42. Bowton E, Saunders C, Erreger K, Sakrikar D, Matthies HJ, Sen N, et al. Dysregulation of dopamine transporters via dopamine D2 autoreceptors triggers anomalous dopamine efflux associated with attention-deficit hyperactivity disorder. J Neurosci. 2010 Apr 28;30(17):6048–57.
43. Thal LB, Tomlinson ID, Quinlan MA, Kovtun O, Blakely RD, Rosenthal SJ. Single Quantum Dot Imaging Reveals PKCβ-Dependent Alterations in Membrane Diffusion and Clustering of an Attention-Deficit Hyperactivity Disorder/Autism/Bipolar Disorder-Associated Dopamine Transporter Variant. ACS Chem Neurosci. 2019 Jan 16;10(1):460–71.
44. Garcia-Olivares J, Baust T, Harris S, Hamilton P, Galli A, Amara SG, et al. Gβγ subunit activation promotes dopamine efflux through the dopamine transporter. Mol Psychiatry. 2017 Dec;22(12):1673–9.
45. Pino JA, Nuñez-Vivanco G, Hidalgo G, Reyes Parada M, Khoshbouei H, Torres GE. Identification of Critical Residues in the Carboxy Terminus of the Dopamine Transporter Involved in the G Protein βγ-Induced Dopamine Efflux. Front Pharmacol. 2021;12:642881.
46. Mergy MA, Gowrishankar R, Davis GL, Jessen TN, Wright J, Stanwood GD, et al. Genetic targeting of the amphetamine and methylphenidate-sensitive dopamine transporter: On the path to an animal model of attention-deficit hyperactivity disorder. Vol. 73, Neurochemistry International. Elsevier Ltd; 2014. p. 56–70.
47. Hong WC, Yano H, Hiranita T, Chin FT, McCurdy CR, Su TP, et al. The sigma-1 receptor modulates dopamine transporter conformation and cocaine binding and may thereby potentiate cocaine self-administration in rats. J Biol Chem. 2017 Jul 7;292(27):11250–61.
48. Egaña LA, Cuevas RA, Baust TB, Parra LA, Leak RK, Hochendoner S, et al. Physical and functional interaction between the dopamine transporter and the synaptic vesicle protein synaptogyrin-3. J Neurosci. 2009 Apr 8;29(14):4592–604.
49. Shekar A, Mabry SJ, Cheng MH, Aguilar JI, Patel S, Zanella D, et al. Syntaxin 1 Ser14 phosphorylation is required for nonvesicular dopamine release. Sci Adv. 2023 Jan 13;9(2):eadd8417.
50. Vaughan RA, Foster JD. Mechanisms of dopamine transporter regulation in normal and disease states. Trends Pharmacol Sci. 2013 Sep;34(9):489–96.

51. Bermingham DP, Blakely RD. Kinase-dependent Regulation of Monoamine Neurotransmitter Transporters. Pharmacol Rev. 2016 Oct;68(4):888–953.
52. Bolan EA, Kivell B, Jaligam V, Oz M, Jayanthi LD, Han Y, et al. D2 receptors regulate dopamine transporter function via an extracellular signal-regulated kinases 1 and 2-dependent and phosphoinositide 3 kinase-independent mechanism. Mol Pharmacol. 2007 May;71(5):1222–32.
53. Zapata A, Kivell B, Han Y, Javitch JA, Bolan EA, Kuraguntla D, et al. Regulation of dopamine transporter function and cell surface expression by D3 dopamine receptors. J Biol Chem. 2007 Dec 7;282(49):35842–54.
54. Kivell B, Uzelac Z, Sundaramurthy S, Rajamanickam J, Ewald A, Chefer V, et al. Salvinorin A regulates dopamine transporter function via a kappa opioid receptor and ERK1/2-dependent mechanism. Neuropharmacology. 2014 Nov;86:228–40.
55. Lee FJS, Pei L, Moszczynska A, Vukusic B, Fletcher PJ, Liu F. Dopamine transporter cell surface localization facilitated by a direct interaction with the dopamine D2 receptor. EMBO J. 2007 Apr 18;26(8):2127–36.
56. Gowrishankar R, Gresch PJ, Davis GL, Katamish RM, Riele JR, Stewart AM, et al. Region-Specific Regulation of Presynaptic Dopamine Homeostasis by D2 Autoreceptors Shapes the In Vivo Impact of the Neuropsychiatric Disease-Associated DAT Variant Val559. J Neurosci. 2018 Jun 6;38(23):5302–12.
57. Luethi D, Liechti ME. Designer drugs: mechanism of action and adverse effects. Arch Toxicol. 2020 Apr;94(4):1085–133.
58. Svingos AL, Chavkin C, Colago EE, Pickel VM. Major coexpression of kappa-opioid receptors and the dopamine transporter in nucleus accumbens axonal profiles. Synapse. 2001 Dec 1;42(3):185–92.
59. Margolis EB, Hjelmstad GO, Bonci A, Fields HL. Kappa-opioid agonists directly inhibit midbrain dopaminergic neurons. J Neurosci. 2003 Nov 5;23(31):9981–6.
60. Land BB, Bruchas MR, Lemos JC, Xu M, Melief EJ, Chavkin C. The dysphoric component of stress is encoded by activation of the dynorphin kappa-opioid system. J Neurosci. 2008 Jan 9;28(2):407–14.
61. Kozono H, Yoshitani H, Nakano R. Post-marketing surveillance study of the safety and efficacy of nalfurafine hydrochloride (Remitch® capsules 2.5 µg) in 3,762 hemodialysis patients with intractable pruritus. Int J Nephrol Renovasc Dis. 2018;11:9–24.
62. Reed B, Butelman ER, Fry RS, Kimani R, Kreek MJ. Repeated Administration of Opra Kappa (LY2456302), a Novel, Short-Acting, Selective KOP-r Antagonist, in Persons with and without Cocaine Dependence. Neuropsychopharmacology. 2018 Mar;43(4):928.
63. Lowe SL, Wong CJ, Witcher J, Gonzales CR, Dickinson GL, Bell RL, et al. Safety, tolerability, and pharmacokinetic evaluation of single- and multiple-ascending doses of a novel kappa opioid receptor antagonist LY2456302 and drug interaction with ethanol in healthy subjects. J Clin Pharmacol. 2014 Sep;54(9):968–78.
64. Krystal AD, Pizzagalli DA, Smoski M, Mathew SJ, Nurnberger J, Lisanby SH, et al. A randomized proof-of-mechanism trial applying the “fast-fail” approach to evaluating κ-opioid antagonism as a treatment for anhedonia. Nat Med. 2020 May;26(5):760–8.
65. Pizzagalli DA, Smoski M, Ang YS, Whitton AE, Sanacora G, Mathew SJ, et al. Selective kappa-opioid antagonism ameliorates anhedonic behavior: evidence from the Fast-fail Trial in Mood and Anxiety Spectrum Disorders (FAST-MAS). Neuropsychopharmacology. 2020 Sep;45(10):1656–63.
66. Foster JD, Yang JW, Moritz AE, Challasivakanaka S, Smith MA, Holy M, et al. Dopamine transporter phosphorylation site threonine 53 regulates substrate reuptake and amphetamine-stimulated efflux. J Biol Chem. 2012 Aug 24;287(35):29702–12.

67. Mowlem FD, Rosenqvist MA, Martin J, Lichtenstein P, Asherson P, Larsson H. Sex differences in predicting ADHD clinical diagnosis and pharmacological treatment. Eur Child Adolesc Psychiatry. 2019 Apr;28(4):481–9.
68. Daws LC, Owens WA, Toney GM. Using High-Speed Chronoamperometry to Measure Biogenic Amine Release and Uptake In Vivo. In 2016. p. 53–81.
69. Paxinos G, Watson C. The Rat Brain in Stereotaxic Coordinates. 6th ed. San Diego: Academic Press; 1998.
70. Horan P, Taylor J, Yamamura HI, Porreca F. Extremely long-lasting antagonistic actions of nor-binaltorphimine (nor-BNI) in the mouse tail-flick test. J Pharmacol Exp Ther. 1992 Mar;260(3):1237–43.
71. Bruchas MR, Yang T, Schreiber S, Defino M, Kwan SC, Li S, et al. Long-acting kappa opioid antagonists disrupt receptor signaling and produce noncompetitive effects by activating c-Jun N-terminal kinase. J Biol Chem. 2007 Oct 12;282(41):29803–11.
72. Mayer FP, Niello M, Cintulova D, Sideromenos S, Maier J, Li Y, et al. Serotonin-releasing agents with reduced off-target effects. Mol Psychiatry. 2023 Feb;28(2):722–32.
73. Ramamoorthy S, Shippenberg TS, Jayanthi LD. Regulation of monoamine transporters: Role of transporter phosphorylation. Pharmacol Ther. 2011 Feb;129(2):220–38.
74. Foster JD, Vaughan RA. Phosphorylation mechanisms in dopamine transporter regulation. J Chem Neuroanat. 2017 Oct;83–84:10–8.
75. Gorentla BK, Moritz AE, Foster JD, Vaughan RA. Proline-directed phosphorylation of the dopamine transporter N-terminal domain. Biochemistry. 2009 Feb 10;48(5):1067–76.
76. Challasivakanaka S, Zhen J, Smith ME, Reith MEA, Foster JD, Vaughan RA. Dopamine transporter phosphorylation site threonine 53 is stimulated by amphetamines and regulates dopamine transport, efflux, and cocaine analog binding. J Biol Chem. 2017 Nov 17;292(46):19066–75.
77. Ragu Varman D, Subler MA, Windle JJ, Jayanthi LD, Ramamoorthy S. Novelty-induced hyperactivity and suppressed cocaine induced locomotor activation in mice lacking threonine 53 phosphorylation of dopamine transporter. Behavioural brain research. 2021 Jun 25;408:113267.
78. Li LB, Chen N, Ramamoorthy S, Chi L, Cui XN, Wang LC, et al. The role of N-glycosylation in function and surface trafficking of the human dopamine transporter. J Biol Chem. 2004 May 14;279(20):21012–20.
79. Gulley JM, Larson GA, Zahniser NR. Using High-Speed Chronoamperometry with Local Dopamine Application to Assess Dopamine Transporter Function. 2007.
80. Volkow ND, Wang GJ, Newcorn J, Fowler JS, Telang F, Solanto M V, et al. Brain dopamine transporter levels in treatment and drug naïve adults with ADHD. Neuroimage. 2007 Feb 1;34(3):1182–90.
81. Howes OD, McCutcheon R, Owen MJ, Murray RM. The Role of Genes, Stress, and Dopamine in the Development of Schizophrenia. Biol Psychiatry. 2017 Jan 1;81(1):9–20.
82. Jeste SS, Geschwind DH. Disentangling the heterogeneity of autism spectrum disorder through genetic findings. Nat Rev Neurol. 2014 Feb;10(2):74–81.
83. Wang YM, Gainetdinov RR, Fumagalli F, Xu F, Jones SR, Bock CB, et al. Knockout of the vesicular monoamine transporter 2 gene results in neonatal death and supersensitivity to cocaine and amphetamine. Neuron. 1997 Dec;19(6):1285–96.
84. Zhou QY, Palmiter RD. Dopamine-deficient mice are severely hypoactive, adipsic, and aphagic. Cell. 1995 Dec 29;83(7):1197–209.
85. Kurian MA, Zhen J, Cheng SY, Li Y, Mordekar SR, Jardine P, et al. Homozygous loss-of-function mutations in the gene encoding the dopamine transporter are associated with infantile parkinsonism-dystonia. J Clin Invest. 2009 Jun;119(6):1595–603.
86. Kurian MA. SLC6A3-Related Dopamine Transporter Deficiency Syndrome. 1993.

87. Azocar VH, Sepúlveda G, Ruiz C, Aguilera C, Andrés ME, Fuentealba JA. The blocking of kappa-opioid receptor reverses the changes in dorsolateral striatum dopamine dynamics during the amphetamine sensitization. J Neurochem. 2019 Feb;148(3):348–58.
88. Thompson AC, Zapata A, Justice JB, Vaughan RA, Sharpe LG, Shippenberg TS. Kappa-opioid receptor activation modifies dopamine uptake in the nucleus accumbens and opposes the effects of cocaine. J Neurosci. 2000 Dec 15;20(24):9333–40.
89. Vaughan RA, Huff RA, Uhl GR, Kuhar MJ. Protein kinase C-mediated phosphorylation and functional regulation of dopamine transporters in striatal synaptosomes. J Biol Chem. 1997 Jun 13;272(24):15541–6.
90. Fog JU, Khoshbouei H, Holy M, Owens WA, Vaegter CB, Sen N, et al. Calmodulin kinase II interacts with the dopamine transporter C terminus to regulate amphetamine-induced reverse transport. Neuron. 2006 Aug 17;51(4):417–29.
91. Kearney PJ, Bolden NC, Kahuno E, Conklin TL, Martin GE, Lubec G, et al. Presynaptic Gq-coupled receptors drive biphasic dopamine transporter trafficking that modulates dopamine clearance and motor function. J Biol Chem. 2023 Feb;299(2):102900.
92. Van't Veer A, Bechtholt AJ, Onvani S, Potter D, Wang Y, Liu-Chen LY, et al. Ablation of kappa-opioid receptors from brain dopamine neurons has anxiolytic-like effects and enhances cocaine-induced plasticity. Neuropsychopharmacology. 2013 Jul;38(8):1585–97.
93. Pomrenze MB, Cardozo Pinto DF, Neumann PA, Llorach P, Tucciarone JM, Morishita W, et al. Modulation of 5-HT release by dynorphin mediates social deficits during opioid withdrawal. Neuron. 2022 Dec 21;110(24):4125-4143.e6.
94. Lycas MD, Ejdrup AL, Sørensen AT, Haahr NO, Jørgensen SH, Guthrie DA, et al. Nanoscopic dopamine transporter distribution and conformation are inversely regulated by excitatory drive and D2 autoreceptor activity. Cell Rep. 2022 Sep 27;40(13):111431.
95. Belovich AN, Aguilar JI, Mabry SJ, Cheng MH, Zanella D, Hamilton PJ, et al. A network of phosphatidylinositol (4,5)-bisphosphate (PIP2) binding sites on the dopamine transporter regulates amphetamine behavior in Drosophila Melanogaster. Mol Psychiatry. 2021 Aug;26(8):4417–30.
96. Hamilton PJ, Belovich AN, Khelashvili G, Saunders C, Erreger K, Javitch JA, et al. PIP2 regulates psychostimulant behaviors through its interaction with a membrane protein. Nat Chem Biol. 2014 Jul;10(7):582–9.
97. Binda F, Dipace C, Bowton E, Robertson SD, Lute BJ, Fog JU, et al. Syntaxin 1A interaction with the dopamine transporter promotes amphetamine-induced dopamine efflux. Mol Pharmacol. 2008 Oct;74(4):1101–8.
98. Buchmayer F, Schicker K, Steinkellner T, Geier P, Stübiger G, Hamilton PJ, et al. Amphetamine actions at the serotonin transporter rely on the availability of phosphatidylinositol-4,5-bisphosphate. Proc Natl Acad Sci U S A. 2013 Jul 9;110(28):11642–7.
99. Lalonde R. The neurobiological basis of spontaneous alternation. Neurosci Biobehav Rev. 2002 Jan;26(1):91–104.
100. Zhang L, McCarthy DM, Eskow Jaunarajs KL, Biederman J, Spencer TJ, Bhide PG. Frontal Cortical Monoamine Release, Attention, and Working Memory in a Perinatal Nicotine Exposure Mouse Model Following Kappa Opioid Receptor Antagonism. Cereb Cortex. 2021 Jan 1;31(1):483–96.
101. Annett LE, McGregor A, Robbins TW. The effects of ibotenic acid lesions of the nucleus accumbens on spatial learning and extinction in the rat. Behavioural brain research. 1989 Jan 1;31(3):231–42.
102. Thifault S, Krémarik P, Lalonde R. Effects of bilateral electrolytic lesions of the medial nucleus accumbens on exploration and spatial learning. Arch Physiol Biochem. 1998 Oct;106(4):297–307.

103. Taghzouti K, Simon H, Hervé D, Blanc G, Studler JM, Glowinski J, et al. Behavioural deficits induced by an electrolytic lesion of the rat ventral mesencephalic tegmentum are corrected by a superimposed lesion of the dorsal noradrenergic system. Brain Res. 1988 Feb 2;440(1):172–6.
104. Pooters T, Laeremans A, Gantois I, Vermaercke B, Arckens L, D'Hooge R. Comparison of the spatial-cognitive functions of dorsomedial striatum and anterior cingulate cortex in mice. PLoS One. 2017;12(5):e0176295.
105. Dwyer JB, Cardenas A, Franke RM, Chen Y, Bai Y, Belluzzi JD, et al. Prenatal nicotine sex-dependently alters adolescent dopamine system development. Transl Psychiatry. 2019 Nov 18;9(1):304.
106. Zhou FM, Liang Y, Dani JA. Endogenous nicotinic cholinergic activity regulates dopamine release in the striatum. Nat Neurosci. 2001 Dec;4(12):1224–9.